Twenty-ninth Canadian Geotechnical Colloquium: The role of advanced numerical methods and geotechnical field measurements in understanding complex deep-seated rock slope failure mechanisms

Erik Eberhardt

Abstract: The underlying complexity associated with deep-seated rock slope stability problems usually restricts their treatment to phenomenological studies that are largely descriptive and qualitative. Quantitative assessments, when employed, typically focus on assessing the stability state but ignore factors related to the slope's temporal evolution including rock mass strength degradation, internal shearing, and progressive failure, all of which are key processes contributing to the final collapse of the slope. Reliance on displacement monitoring for early warning and the difficulty in interpreting the data without a clear understanding of the underlying mechanisms has led to a situation where predictions are highly variable and generally unreliable. This paper reviews current knowledge regarding prefailure mechanisms of massive rock slopes and current practices used to assess the hazard posed. Advanced numerical modelling results are presented that focus on the importance of stress- and strain-controlled rock mass strength degradation leading to failure initiation. Efforts to address issues related to parameter and model uncertainty are discussed in the context of a high alpine research facility, the "Randa In Situ Rockslide Laboratory", where state-of-the-art instrumentation systems and numerical modelling are being used to better understand the mechanisms controlling prefailure deformations over time and their evolution leading to catastrophic failure.

Key words: rock slope stability, progressive failure, numerical modelling, shear strength reduction, slope monitoring, data integration.

Résumé : La complexité sous-jacente associée aux problèmes de stabilité profonde de pentes rocheuses oblige habituellement à en limiter le traitement aux études phénoménologiques qui sont principalement descriptives et qualitatives. Les évaluations quantitatives, lorsqu'utilisées, se concentrent typiquement sur l'évaluation de l'état de stabilité mais ignore les facteurs reliés à l'évolution temporelle incluant la dégradation de la résistance du massif rocheux, le cisaillement interne et la rupture progressive, tous ces processus étant des phénomènes clés contribuant à la rupture finale de la pente. La fiabilité des mesures de déplacement pour une alerte précoce et la difficulté d'interprétation des données sans une compréhension claire des mécanismes sous-jacents a conduit à une situation où les prédictions sont hautement variables et généralement non fiable. Cet article revoit les connaissances courantes sur les mécanismes prérupture des pentes de roc massif et les pratiques courantes utilisées pour évaluer les risques qui se présentent. On présente une modélisation numérique avancée des résultats qui se concentre sur l'importance de la dégradation de la résistance à contrainte et à déformation contrôlées du massif rocheux conduisant à l'initiation de la rupture. On discute des efforts pour traiter les problèmes reliés à l'incertitude des paramètres et du modèle dans le contexte d'une installation de recherche dans les hautes Alpes, le « Randa In Situ Rockslide Laboratory », où des systèmes d'instrumentations selon les règles de l'art et une modélisation numérique sont utilisés pour mieux comprendre les mécanismes contrôlant les déformations de prérupture dans le temps et leur évolution conduisant à une rupture catastrophique.

Mots-clés : stabilité de pente rocheuse, rupture progressive, modélisation numérique, réduction de la résistance au cisaillement, mesure de la pente, intégration des données.

[Traduit par la Rédaction]

Introduction

Globally, a massive rock slope failure involving a volume exceeding 20 million cubic metres occurs every 2.7 years (Evans 2006). These events have been responsible for some of the most destructive natural disasters in terms of human and material losses. With ever-increasing population growth throughout the world's mountainous regions, and therefore increasing societal exposure to rock slope hazards, experts are being called upon to analyse and predict – assessing po-

Received 30 October 2006. Accepted 31 October 2007. Published on the NRC Research Press Web site at cgj.nrc.ca on 23 April 2008.

E. Eberhardt. Geological Engineering – Earth and Ocean Sciences, 6339 Stores Road, The University of British Columbia, Vancouver, BC V6T 1Z4, Canada. (e-mail: erik@eos.ubc.ca).

 doi:10.1139/T07-116

tential modes of failure, risk, and possible preventive and (or) remedial measures.

Our ability to do so, however, is limited by the descriptive and qualitative nature of most analyses, many of which tend to provide only minimal insight into the underlying processes and mechanisms driving instability and failure. The degree to which prediction is achievable is also contentious, with many seeing it as being limited to the assessment of stability (i.e., factor of safety). Prediction of failure with respect to time, which is what society asks from us, seems distant as we try to contend with the large number of unknowns, uncertainties, and complexities associated with the subsurface geology, hydrogeology, and superimposition of triggering events.

In answer to these challenges, advances in engineering tool development are continuously being made with much focus being placed on numerical modelling. Numerical modelling provides a powerful means to analyze complex rock mass interactions and rock slope stability states as a function of changing environmental factors. However, such analyses require tight controls on boundary conditions, material properties, and rock mass constitutive relationships, leading detractors to exclaim "garbage in, garbage out" in the absence of detailed field mapping or monitoring data to constrain the analyses with. At the same time it must be recognized that most in situ measurements are affected by the same issues of rock mass complexity and variability as the numerical analyses they are meant to constrain. The presence of persistent and nonpersistent discontinuities, multiple moving blocks, and internal shear surfaces (e.g., Figure 1) impose a significant complexity making the interpretation of rock slope monitoring data especially difficult. The questions that follow then are whether geotechnical field measurements are just as suspect as the models they are meant to constrain and calibrate and whether numerical models in return could be used to aid in their interpretation (Eberhardt and Willenberg 2005).

Instead of focusing on the limitations of a specific tool, this places the emphasis on how the tools that are available to us as practitioners are used, and more importantly, integrated within the overall hazard assessment. By better integrating the different data sets and analysis output available, geological uncertainty can be minimized and better managed so as to aid critical thinking and engineering judgement.

This paper examines the use and integration of numerical modelling and field-based geotechnical measurements to provide key insights into deep-seated rock slope failure mechanisms. The first part of the paper concentrates on the question of prediction. Spatial prediction is examined in the context of a "total slope analysis" (Stead et al. 2006), using numerical techniques to assess the stability state, potential volume(s), and runout paths and distances in the event of catastrophic failure. Temporal prediction is discussed focusing on the limitations of empirical treatments of slope monitoring data for early warning and the need for improved consideration of the mechanisms and processes involved. The second part of the paper addresses the issue of improved understanding of rock slope failure mechanisms by outlining the lessons learned from a unique series of numerical- and field-based experiments designed to improve our understanding of prefailure deformation processes in brittle crystalline rock masses – the Randa study (carried out in the Swiss Alps). The importance of strength degradation and progressive failure under different rock slope stress and relaxation conditions are presented based on numerical models of the 1991 Randa rockslide events. These include the use of new "state-of-the-art" numerical tools to develop a better understanding of the mechanistic role extensional strain and brittle fracture processes play in the evolution of massive rock slope failure. With these are presented a summary of some key findings from the experimental work carried out for the present-day instability at Randa in the form of the "Randa In Situ Rockslide Laboratory", a high-alpine facility involving the integration of instrumentation systems designed to measure three-dimensional (3-D) spatial and temporal relationships among fracture systems, displacements, pore pressures, and microseismicity.

Rock slope hazard prediction

Total slope analysis

The assessment of the hazard posed by a large unstable rock slope requires information on several key factors:

- state of stability (i.e., factor of safety and (or) probability of failure);
- anticipated failure mechanism;
- potential failure volume;
- extent of warning prior to failure;
- deformation behaviour at failure; and
- post-failure runout distance and velocity.

In practice, these factors are assessed based on experience and comparison with precedents, aided by analytical and (or) empirical analyses (Hungr et al. 2005). In most cases they are treated separately but are linked by a common requirement to be constrained by detailed geological and geotechnical field observations.

Stead et al. (2006) propose though that analyses relating to failure initiation need not be treated separately from those relating to transport and deposition (i.e., runout analysis). Instead, with the use of advanced numerical models, they can be linked together as a total slope analysis, where the deformation characteristics and kinematics prior to failure are used to help model the post-failure movement and dynamics. This can be further extended to link back analyses of an earlier failure (where applicable) to forward predictive models, enabling the results from each step to be used to provide important insights, mechanistic controls, and parameter constraints for subsequent steps in the hazard assessment (Fig. 2). These include results, for an anticipated mode of failure, relating to the rock slope stability state (including its sensitivity to different environmental factors) and the potential extent, depth, and volume of failure.

Stability state, factor of safety, and shear strength reduction

The assessment of a rock slope's stability state is commonly quantified in terms of a factor of safety (the balance between resisting and disturbing forces), calculated using one of a number of closed-form or iterative limit equilibrium solutions depending on the anticipated mode of failure. Distinction is made between structurally controlled failure, where solutions are restricted to toppling or shear

Fig. 1. Rock slope instability mechanisms as controlled by persistent and nonpersistent discontinuities and internal rock mass deformation and shearing (after Eberhardt et al. 2004*a*).

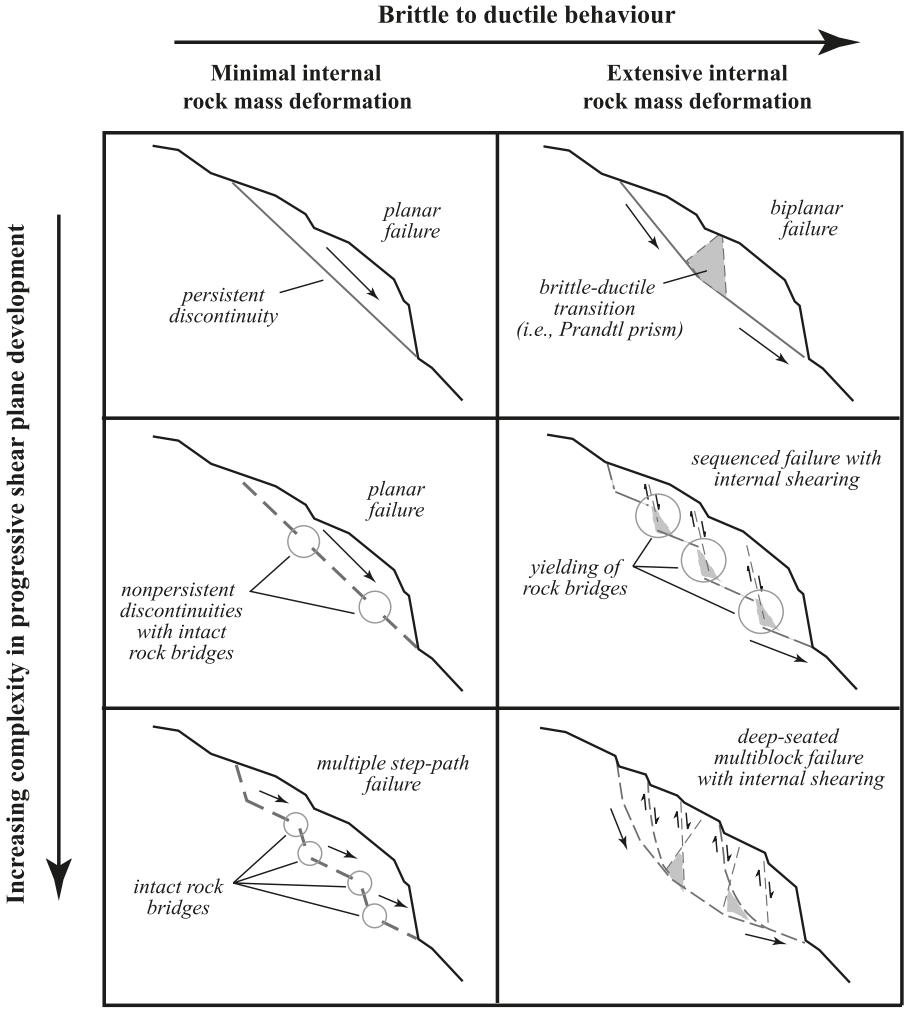

along intersecting discontinuities (determined beforehand using stereonet techniques; e.g., Wyllie and Mah 2004), and stress-controlled failure where solutions apply to shear failure through an equivalent rock mass continuum (e.g., method of slices; see Fredlund and Krahn 1977). In the case of the latter, critical shear surface search routines assuming either circular or noncircular slip surfaces are used to find the most likely path of failure. When combined with precipitation and infiltration records, results from a limit equilibrium analysis can be used to determine trigger thresholds for which case-specific predictions of depth and relative time of failure can be made (Collins and Znidarcic 2004). Similar threshold studies have been performed for earthquake triggering (e.g., Shou and Wang 2003). Correlations to triggering mechanisms and their repeat frequency represent one of the few means by which analytical approaches can be used for temporal predictions. Confidence in these predictions, however, may be limited by the degree of model and parameter uncertainty involved, and instead often serve better when combined with other analyses to define early warning thresholds relating to different hazard levels.

To deal with issues of parameter uncertainty, probabilistic tools are more frequently being used in combination with limit equilibrium analyses. Instead of calculating a single factor of safety for a slope, a distribution of safety factors is calculated (Fig. 3) from repeated iterations of the stability model using different combinations of input parameters selected from their credible ranges by Monte Carlo sampling techniques (see also Lee and Jones 2004). The "probability of failure" is then computed as the percentage of analyses performed where the factor of safety was less than 1.0. A "reliability index" follows as the number of standard deviations separating the mean factor of safety from the critical value of 1.0. These parameters provide a measure of the uncertainty involved in the results of the analysis and thus in that of the stability state of the slope. Reliability concepts can then be applied to provide a logical framework for choosing factors of safety that are appropriate for the degree of uncertainty and the consequences of failure involved (Duncan 2000). It should be noted, however, that probabilistic limit equilibrium analyses assume that parameter variability is the only source of uncertainty, neglecting issues related to sampling uncertainty (do our samples represent the parameters correctly) and model uncertainty (is our model of the failure mechanism correct).

In a total slope analysis, limit equilibrium analyses should

Fig. 2. "Total slope analysis" linking field data collection and back analyses of failure initiation and runout, to forward predictive analyses.

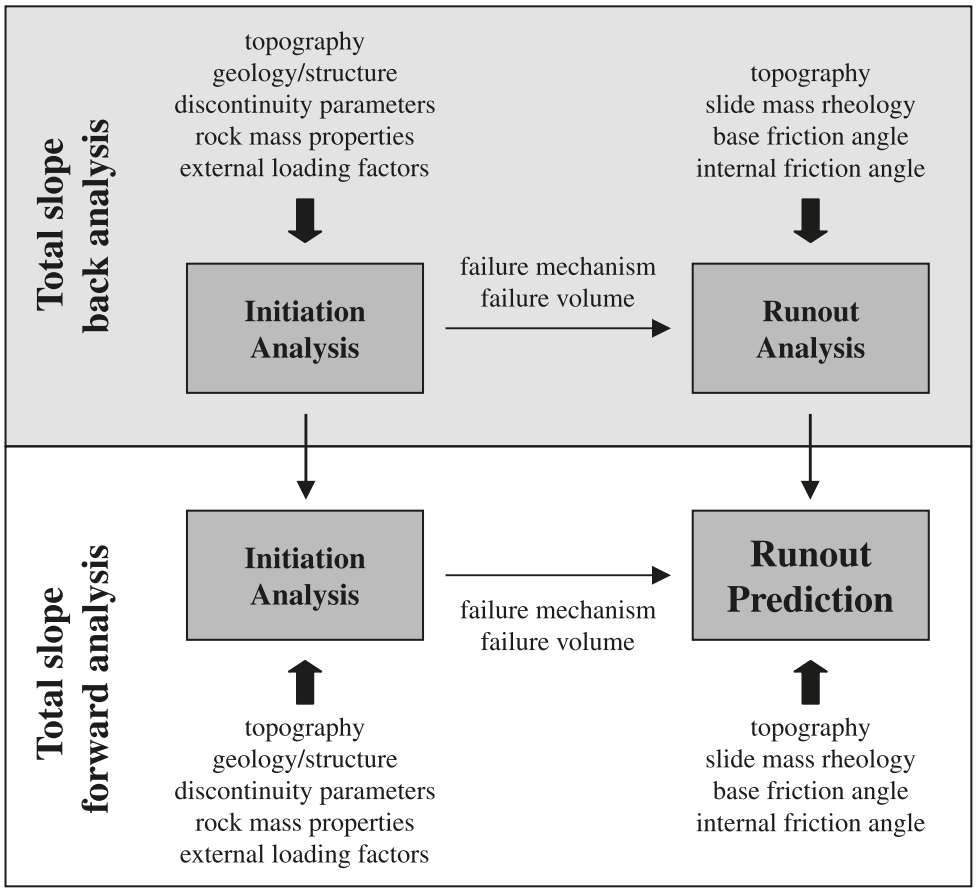

Fig. 3. Rock slope stability states expressed as a function of the factor of safety and its probability distribution (after Brunsden 1979).

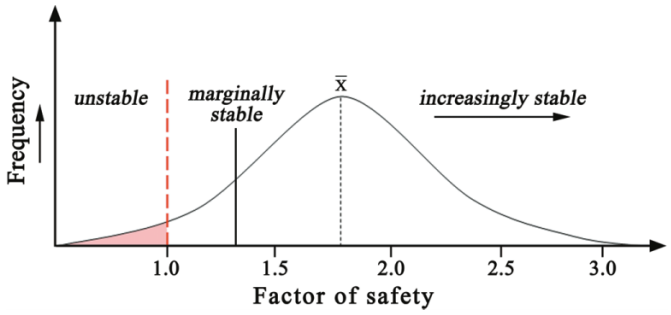

be followed by detailed numerical analyses to investigate and better understand the underlying mechanisms controlling the instability, thus helping to reduce model uncertainty. Numerical methods employ stress–strain constitutive relationships, which allow for the modelling of prefailure deformation and its control on strength degradation processes, yield, and shear surface localization and development. Distinction is again made between discontinuum-based techniques (e.g., distinct-element method) and those adhering to an equivalent continuum (e.g., finite-difference or finite-element). The technique(s) chosen depends on both the site conditions and the potential mode of failure, with careful consideration being given to the varying strengths, weaknesses, and limitations inherent in each methodology (see Stead et al. 2006). High quality data enables the objectives to focus more on prediction (i.e., forward modelling of a potential instability), whereas limited data may restrict the analysis to establishing and understanding the dominant mechanisms that may affect the behaviour of the system.

Recent developments have also seen the shift towards using numerical methods to calculate the factor of safety through shear strength reduction (SSR) techniques, primarily for deeper-seated modes of failure. Shear strength reduction involves a procedure whereby the shear strength of the soil or rock is reduced until collapse occurs, from which a factor of safety is produced by comparing the estimated shear strength of the material to the reduced shear strength for failure. Adopting a Mohr–Coulomb yield condition, the factor of safety is defined according to the equations

$$[1] \qquad c^{\text{trial}} = \frac{1}{F_{\text{trial}}}\, c$$

$$[2] \qquad \phi^{\text{trial}} = \arctan\left(\frac{1}{F_{\text{trial}}}\tan\phi\right)$$

where the factor of safety equals the value of the factor F_{trial} by which cohesion, c, and the friction angle, ϕ, are adjusted to bring the model to failure (Dawson et al. 1999). This definition of the factor of safety is exactly the same as that

Fig. 4. Mesh dependency of shear strain localization and factor of safety calculated using the finite-difference shear strength reduction (SSR) technique. Model geometry and initial material properties are the same for each case (density is equal to 2600 kg/m^3, cohesion, c = 1 MPa, and friction angle, $\phi = 40°$).

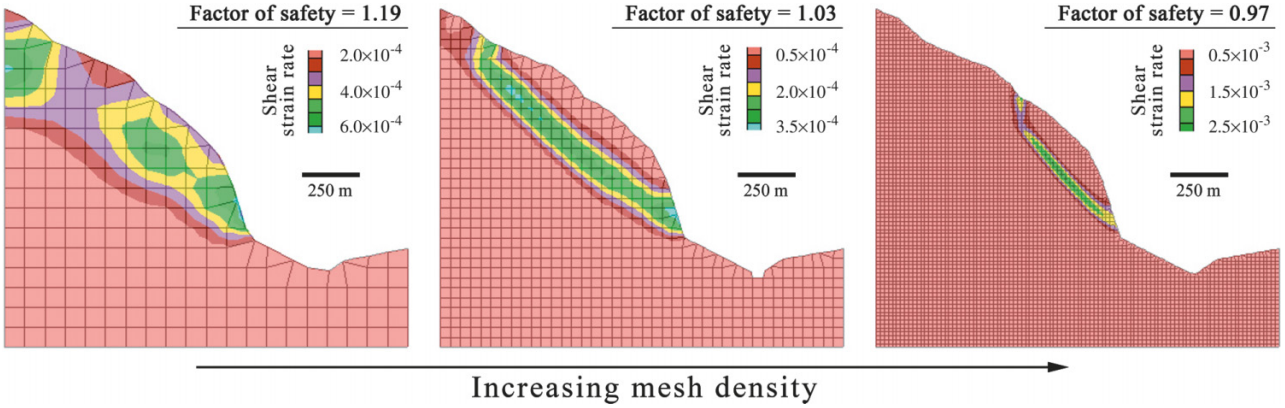

used in traditional limit equilibrium methods (Griffiths and Lane 1999).

The advantage of the SSR technique over limit equilibrium solutions is that it allows the critical slip surface to be automatically found as a function of the stress state and elastoplastic yielding (Dawson et al. 1999). Wong (1984) notes though, that this same versatility hinders the applicability of the technique as there is no clear indicator of failure such as that explicitly expressed through the factor of safety relationship. Instead, a numerical definition of failure must be adopted. Several have been forwarded with the most widely accepted being that of nonconvergence of the solution where iterative procedures are used to solve the force equilibrium equations. Zienkiewicz (1971) suggested that a lack of convergence in such cases can usually be attributed to collapse of the structure. Thus, the basic algorithm for the SSR technique applied using the finite element method involves incrementally increasing the value of F^{trial} in eqs. [1] and [2] until the solution no longer converges; if the slope properties initially produce an unstable state, then the value of F^{trial} is incrementally reduced until the solution converges.

This is the SSR algorithm employed by most commercial finite-element codes, including the widely used rock engineering code Phase^2 (Rocscience 2006). Also widely used, is the commercial finite-difference code FLAC/Slope (Itasca 2005); the FLAC/Slope SSR algorithm differs slightly in that the convergence criterion is related to the nodal unbalanced forces, where a simulation is said to have converged if the normalized unbalanced force of every node is less than 10^{-3} (Dawson et al. 1999).

In applying these codes, parameter uncertainty is still an issue. The factor of safety is still only as accurate as the in situ shear strength properties of the rock–soil mass can be known (as is the case with limit equilibrium). Several sources of model uncertainty also arise, although once understood, are easier to contend with. The first is that the factor of safety calculated is sensitive to the mesh density (e.g., Fig. 4). Shear strain localization is dependent on the size of the elements, for which mesh refinement results in a smaller width of the localization band. This requires that for most cases, as fine a mesh as possible should be used (respecting practical constraints related to solution times) and (or) the mesh sensitivity of the calculated factor of safety be tested. The second key source of model uncertainty is related to the use of nonconvergence to denote failure. In most cases, an elastoplastic constitutive criterion is favoured due to the sudden transition to a yielded state, producing nonconvergence (as used by finite-element SSR algorithms) or a sharp break in the unbalanced forces (as used by finite-difference SSR algorithms). Constitutive models that exhibit a smooth transition from elastic to plastic behaviour result in greater uncertainty and difficulty in identifying the limit state (Dawson et al. 1999).

A third source of model uncertainty relates to the flexibility offered to the user by different commercial codes in terms of which material properties to include in the SSR procedure. Some codes (e.g., Phase^2) follow the technique first applied by Zienkiewicz et al. (1975) in which c and $\tan\phi$ are reduced in the same proportion with each strength reduction step. Other codes (e.g., FLAC/Slope) provide the option to reduce only c or $\tan\phi$, holding the other parameter constant, or to include tensile strength, T_o, and (or) the dilation angle, ψ. Depending on the objectives and experience of the user, these options may prove useful. However, care must be taken in understanding how these different parameters influence the shape of the strength envelope during the strength reduction procedure, and consequently, the shape of the critical slip surface that develops. Figure 5 shows the results of a finite-difference analysis for which either cohesion, friction or both are included in the SSR procedure. Each variant produces a different failure surface. When only the friction angle is reduced, a deeper seated failure surface develops as the Mohr–Coulomb failure envelope intersects stress circles at higher levels of stress (Fig. 5*b*); failure occurs where the stresses are highest in the model – deep below the surface. The situation where only cohesion is reduced (Fig. 5*c*) produces a shallow failure because the Mohr–Coulomb failure envelope will first intersect stress circles representing lower levels of stress. In general, the strength reduction technique is more sensitive to changes in cohesion than to changes in the friction angle. Care should be taken when exercising the added flexibility provided by such program options, with consideration being given to the nature of the rock mass and mode of failure (i.e., brittle versus ductile).

Fig. 5. Finite-difference shear strength reduction (SSR) results showing change in the nature of the critical shear surface that develops as a function of: (*a*) both cohesion and friction being reduced; (*b*) only friction being reduced; and (*c*) only cohesion being reduced. Model geometry and initial material properties are the same for each case (density is equal to 2600 kg/m^3, c = 2.5 MPa, ϕ = 40°).

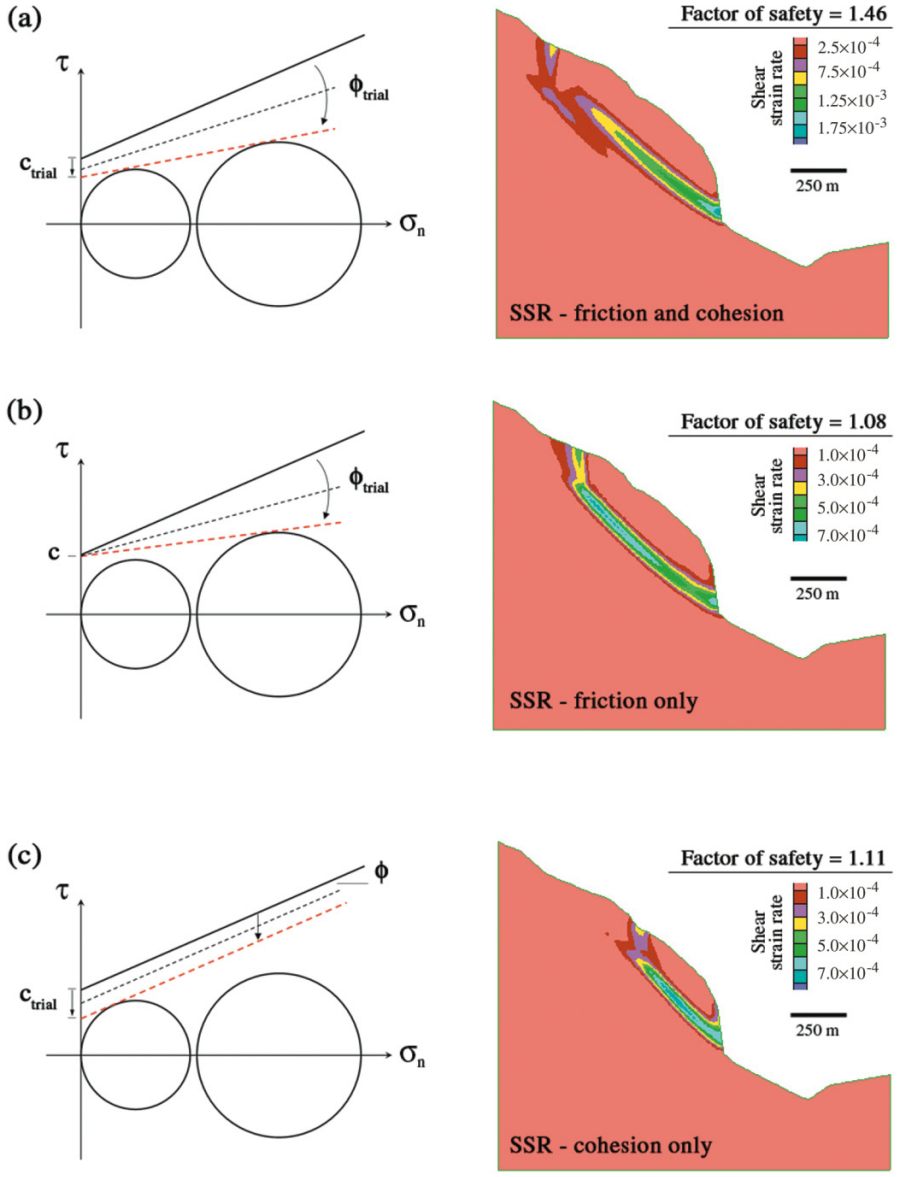

Volume estimates for runout predictions

Once the stability state and failure mechanisms have been established, the focus of the total slope analysis shifts to the use of empirical and analytical methods to assess the potential travel distance and impact velocity of a rockslide event in the event of catastrophic failure. This is referred to as a runout analysis (see Hungr et al. 2005). The key inputs required include the volume of the slide mass and the local morphology of the runout path; the latter being obtainable from surficial geology maps and 3-D digital elevation models. Estimates of the potential failed–released volume can be more difficult. Preliminary estimates are often based on geological interpretations, observations of surface tension cracks, and (or) the local topography, for example, using simple geomorphologic techniques like the sloping local base level (SLBL) method of Jaboyedoff et al. (2005) where the basal sliding surface is estimated through interpolations of the valley bottom and topographic lows along the slope profile. The total slope analysis approach can improve on these estimates by incorporating the results derived from limit equilibrium and numerical stability analyses (Fig. 2), which include predictive quantitative details on the depth and shape of the failure surface. For example, continuum-based numerical methods (e.g., finite-element, finite-difference, etc.) allow the location and shape of the failure surface to progressively develop during the analysis based on the elastic–plastic transition of groups of elements as they pass from an initial linear elastic state to an ultimate state of plastic yield. No commitment is required in the analysis as to any particular form of the failure surface a priori (Griffiths and Lane 1999). The treatment of a rock mass as an equivalent continuum of course discounts the explicit role of discontinuities in controlling the specific path taken by the rupture surface. However, in cases where the discontinuities are nonpersistent and

Fig. 6. Hazard assessment of an unstable rock slope in southern Switzerland, showing: (*a*) signs of active slope instability; (*b*) geological section; (*c*) finite-difference modelling results used to constrain the shape and location of the critical shear surface and estimates of the potential rockslide volume for subsequent runout analyses (see Fig. 7). After Willenberg et al. (2004*a*).

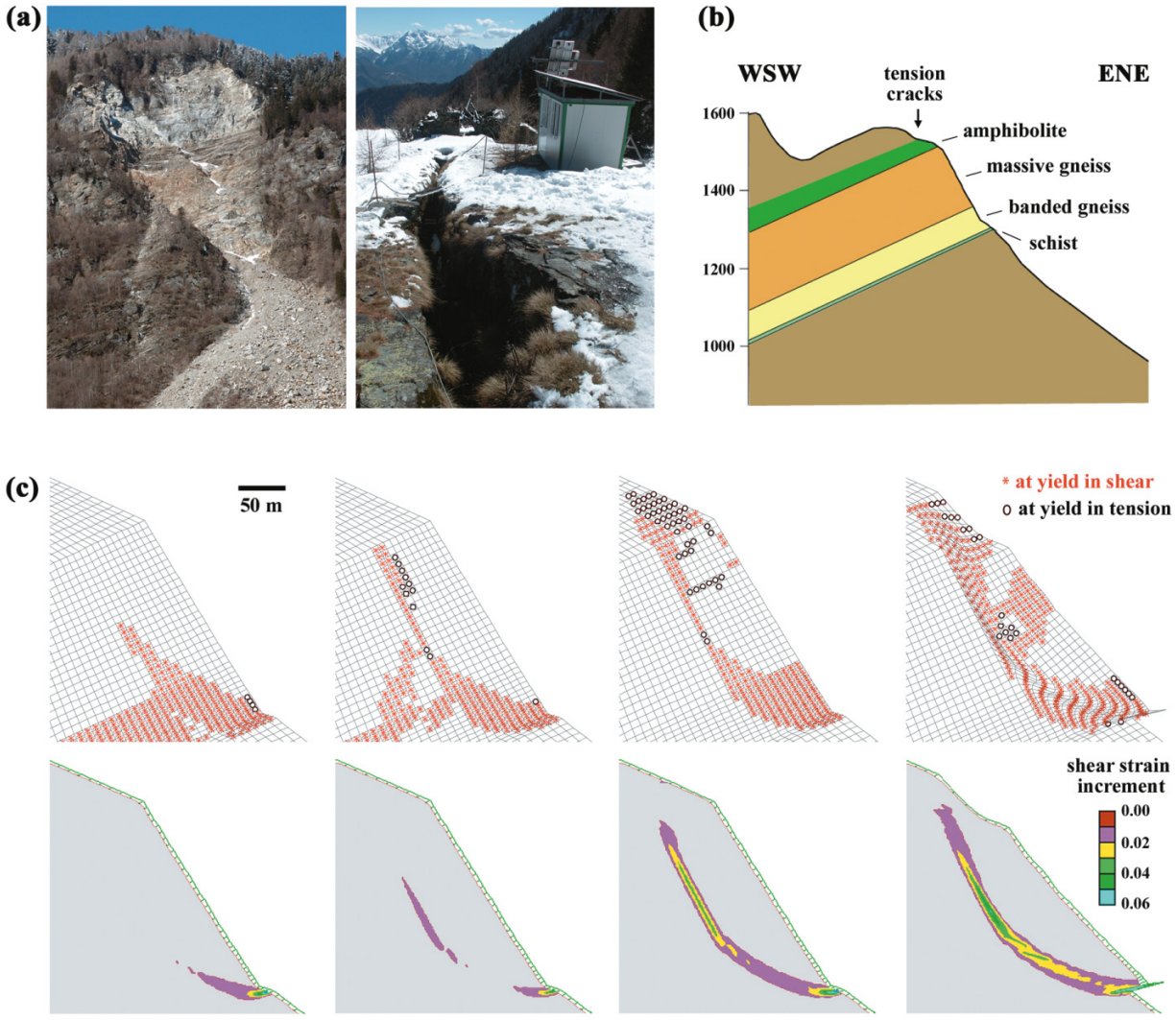

serve more to form step paths as part of a deeper seated rupture surface, as opposed to being highly persistent (e.g., bedding planes) and contributing towards a translational mode of failure, continuum modelling has been shown to be highly effective in reproducing or providing a prediction of the depth of failure (e.g., Eberhardt et al. 2004*a*; Willenberg et al. 2004).

Figures 6 and 7 provide an example of a total slope analysis taken from southern Switzerland, in which a forward prediction of potential rockslide volume was required to perform a runout analysis to assess the risk to several important industrial buildings in the valley below (Fig. 7*a*). The model was solved using a strain softening elastoplastic constitutive model (decreasing strength as a function of increasing plastic strain; e.g., Lo and Lee 1973). The data available for the assessment were limited to those collected through geological mapping and field observations (Willenberg et al. 2004). From this, the surface topography and geology were used to construct the model, and the locations of tension cracks at the top of the slope were used to constrain the model results (Figs. 6*a* and 6*b*). Figure 6*c* shows the modelled results of the shape and location of the critical shear surface, largely controlled by a weak schist layer, from which estimates of the potential rockslide volume were made. These estimates were then used as input to forward model the rockslide runout in the event of catastrophic failure (Figs. 7*b* and 7*c*) using the dynamic analysis code DAN (Hungr 1995).

A second means by which numerical modelling results from the stability analysis can further contribute to the integrated runout analysis is by providing insights into how different processes and mechanisms relating to failure initiation and development extend to influence release of the failed material and runout. These include the likely mode of failure and suddenness of release (brittle, ductile, self-stabilizing, etc.), and whether the rockslide will occur as a single large-volume event or in episodic stages involving smaller release volumes (e.g., Eberhardt et al. 2004*a*). In some cases, this assessment may warrant the use of more than one numerical methodology during the stability analysis. The distinct-element code UDEC (Hart 1993) particularly, has been widely employed for a range of rock slope failure mechanisms: simple planar–translational mech-

Fig. 7. Dynamic runout analysis for different values of basal friction, carried out as part of a total slope analysis using estimated rockslide volumes derived from a slope stability analysis (see Fig. 6). After Willenberg et al. (2004).

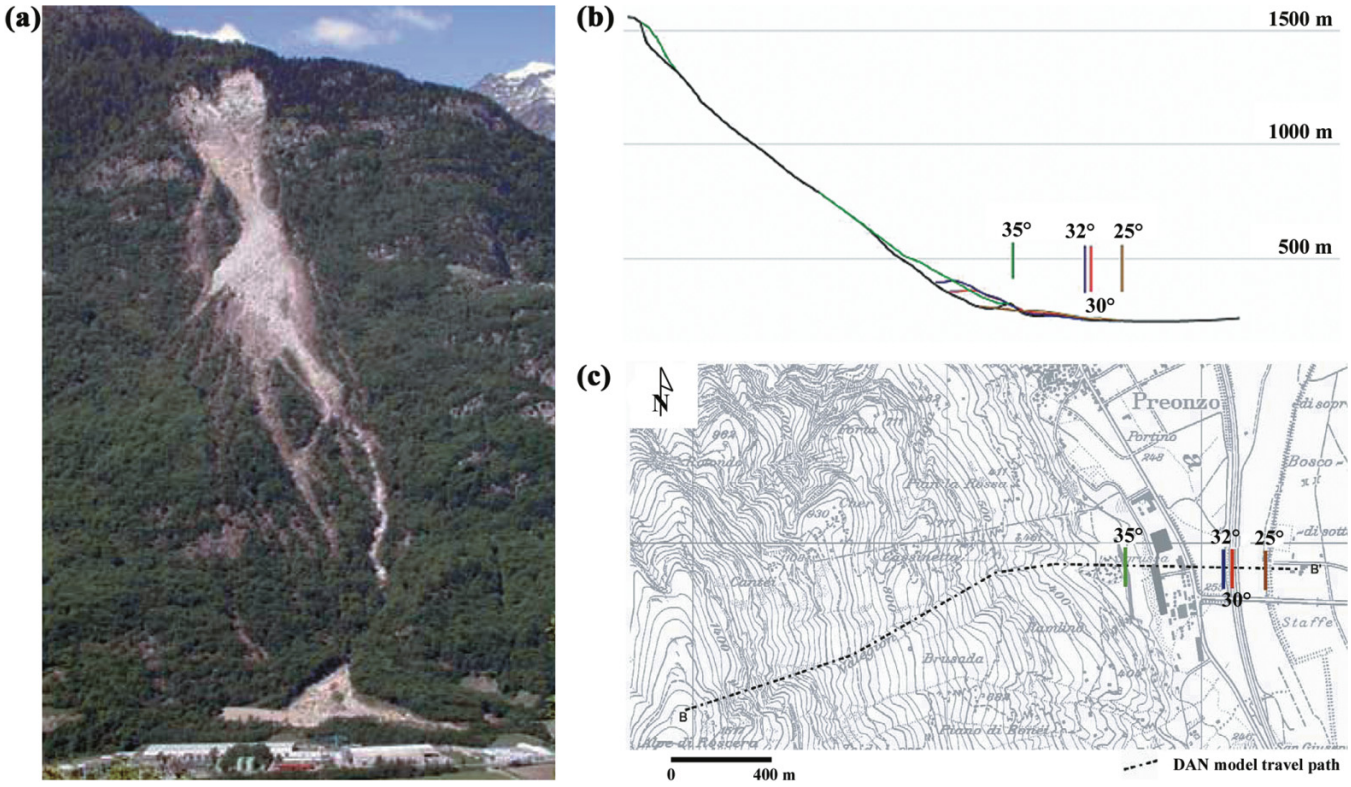

anisms (Costa et al. 1999; Eberhardt et al. 2005), complex deep-seated sliding–rotation (Chryssanthakis and Grimstad 1996; Bhasin and Kaynia 2004), toppling (Board et al. 1996; Nichol et al. 2002), and biplanar, buckling, and ploughing in bedded rock slopes (Stead and Eberhardt 1997). In each of these cases, the modelling results show different characteristics relating to the initiation and development of the failure in the model, which can be equated to different release characteristics upon catastrophic collapse and runout of the slide mass.

An example is provided by Strouth (2006) for a rock slope hazard that threatens a state highway in northern Washington State (Fig. 8). The total slope analysis performed involved a detailed site investigation focusing on both the characterization of the existing threat and that of an earlier rockslide involving 750 000 m^3 of jointed orthogneiss (Fig. 8*a*; see also Strouth et al. 2006). Specific data sets were targeted to provide input for a series of 2-D and 3-D limit equilibrium, distinct-element and dynamic runout analyses, including those collected through both outcrop mapping and terrestrial laser or light detection and ranging (LiDAR) scanning (Fig. 8*b*; Strouth and Eberhardt 2006). The latter enables measurement of discontinuity orientation, spacing and persistence at key, but inaccessible, slope exposures. Back analyses of the earlier slope failure and rockslide runout were carried out (Figs. 8*c* and 8*d*, respectively) to guide forward analyses of the present-day threat and to reduce uncertainty regarding the physical properties (i.e., following the procedure outlined in Fig. 2). Of special concern was the influence of a sharp ridge near the crest of the instability that, depending on the failure mechanism, could direct the released rock down one of two different travel paths (labelled Afternoon Creek and Falls Creek in Fig. 8*a*). This was the case for the earlier failure where the rockslide debris that impacted the highway involved less than 10% of the total failed volume, but had travelled down a steeper path on the opposite side of the ridge from that where most of the slide debris came to rest. Using the 3-D dynamic runout code DAN-3D (McDougall and Hungr 2004), this partitioning of the slide mass could be replicated in the back-analysis of the runout (Fig. 8*d*). For the forward analysis and hazard assessment, the stability state and lower–upper limits of the potential rockslide volume were calculated using a combination of limit equilibrium and distinct element analyses (e.g., Fig. 8*e*), which in turn were used to constrain the post-failure dynamic analysis of the runout path, runout distance, and velocity (Fig. 8*f*).

Empirical approaches to temporal prediction (displacement versus time)

One of the key factors missing from the total slope analysis, and the methods used to assess an unstable rock slope's stability state, is the treatment of time to failure. The constitutive relationships used in most numerical analyses solve for stress, strain, and displacements, but not for time. The application of time-dependent constitutive relationships (e.g., viscoplastic creep) to rock slope stability problems has not yet been fully established. Parameter and model uncertainty provide a major obstacle given the complexity and detailed data requirements such predictions would involve. Several studies have begun though, to investigate the applicability of viscoplastic constitutive models to jointed rock

Fig. 8. Example of a "total slope analysis" applied to a hazardous rock slope in Washington State, showing: (*a*) an earlier rockslide that impacted the state highway below (SR20); (*b*) discontinuity data derived from outcrop mapping and terrestrial LiDAR; (*c*) 3-D distinct-element back-analysis of an earlier rockslide event showing the underside of the modelled failed volume; (*d*) 3-D dynamic runout back-analysis of an earlier rockslide event; (*e*) distinct-element forward analysis of potential rockslide volume; and (*f*) 3-D dynamic runout analysis of potential rockslide runout path and impact velocities threatening the highway. After Strouth (2006).

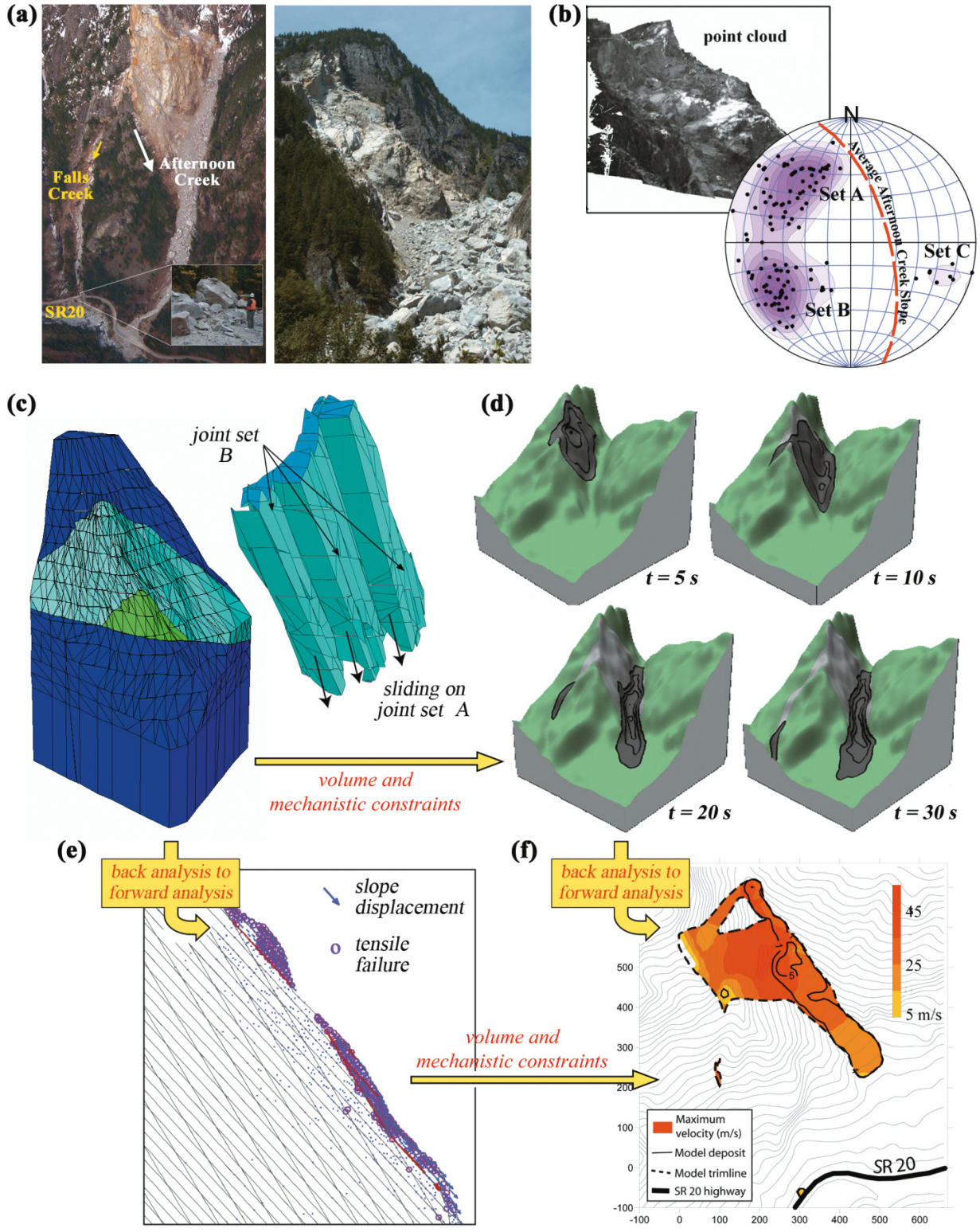

Fig. 9. Illustration of accelerating slope movements that precede failure, correlated to the factor of safety (after Terzaghi 1950).

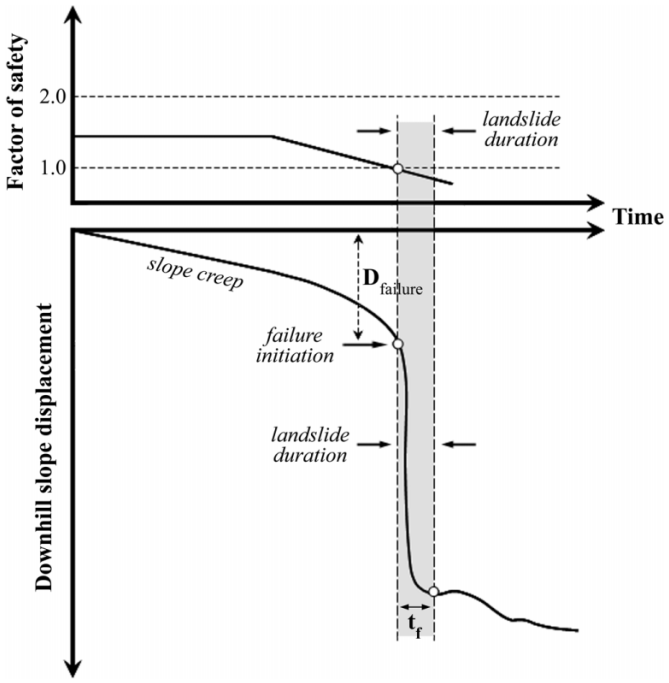

masses and rock slope deformations through distinct-element formulations (e.g., Feng et al. 2003). Distinction must be made between continuous creep involving viscoplastic flow of the rock under constant stress levels, and small cyclic–episodic "stick–slip" movements along existing discontinuities and shear surfaces driven by changing environmental conditions (e.g., fluctuating pore pressures; Bonzanigo et al. 2007). For many deep-seated rock slope instabilities, both are present, but the latter dominates in terms of measured displacements.

Viewed over a long enough period of time, measured rock slope displacements may take the form of a standard creep curve, wherein accelerating slope displacements are taken as a warning of imminent failure (Fig. 9). This technique was applied already by Heim (1932) for a rock slope above the town of Linthal in the Swiss Alps (Kilchenstock), for which two separate forecasts were made predicting catastrophic failure of the slope, neither of which came to pass (Fig. 10; Löw). Heim reported that "lack of experience" was the reason for the inaccurate prediction. Later work by Saito (1965), attempted to compare slope displacement records with constant strain rate and creep rupture curves determined through laboratory testing to predict the time of slope failure. Fukuzono (1985) followed describing relationships between the inverse velocity of slope displacement and failure (e.g., linear, convex, and concave). In the case of the linear relationship, Fukuzono suggested that the time of failure could be predicted by the point where the extrapolated line intersected the time axis (Fig. 11).

Few cases, however, have been reported where these techniques have been successfully applied as part of a forward prediction; most involve back analyses. Some notable exceptions (involving unstable rock slopes) include:

- Kennedy and Niermeyer's (1970) prediction of a major slope failure at the Chuquicamata Mine 5 weeks in advance. The prediction was based on calculations involving the fastest moving monitoring point, and it allowed the rockslide to be designed and worked around such that production was stopped for only 65 h.
- Zvelebil's (1984) report of a toppling failure in sandstones that threatened a highway in the former Czechoslovakia but was safely closed based on predictions made 2 months in advance. The prediction was based on measured displacement rates and the calculated displacements required for overturning of the blocks.
- Rose and Hungr's (2007) accounting of three large pit slope failures in the United States that were predicted 5–90 days in advance, depending on the case. Predictions were based on wireline extensometer and total station survey data analyzed using Fukuzono's inverse velocity method.

Rose and Hungr (2007) note that a number of factors may influence displacement rates and velocity trends prior to failure, including measurement errors, instrument "noise", localized movement, and periodic perturbations (e.g., precipitation, snowmelt, mining activity, etc.). Empirical treatments by nature are "holistic", disregarding the underlying mechanisms and controlling processes while concentrating on the overall behaviour of the system. Whether the displacement measurements are made using extensometers–crackmeters across individual tension cracks or a system of geodetic reflectors covering an entire slope, the technique is applied in the same manner. These factors serve to add a significant degree of ambiguity and subjectivity into the interpretation of the measured data trends. As such, failure forecasts may differ by an order of magnitude for different monitoring devices and (or) locations on the same unstable rock slope (e.g., Crosta and Agliardi 2003). To contend with this, Rose and Hungr recommend that data should be linearly extrapolated over varying lengths of time, looking for a consistent trend and noting and re-evaluating any departures from it, combined with observation of various controlling factors and the developing failure mechanism. Thus, longer-term predictions are never entirely definite and monitoring needs to be continued up to the point of failure.

Despite such deficiencies, displacement monitoring and empirical analysis form an important component of most early warning strategies, where alarm thresholds are set to bring attention to any sudden changes in slope velocity that may serve as a precursor for rapid mobilization (e.g., Salt 1988; Crosta and Agliardi 2003). The prevalent use of displacement monitoring also addresses certain economic realities in terms of what is typically feasible for on-site monitoring of a given rock slope. What appears to be missing, though, is the integration of other analysis tools to help better interpret the nature of the slope displacement signal being recorded – that is, only so much can be inferred from surface monitoring when the problem itself takes place at depth. For most rock slope instabilities, the presence of discontinuities, multiple moving blocks, and internal shear surfaces imposes a significant complexity making the interpretation of slope monitoring data especially difficult.

Figure 12 provides an example of several different modes of rock slope failure commonly encountered in western Canadian coal mines, as controlled by the orientation of

Fig. 10. Early attempt at slope failure forecasting at Kilchenstock, for the town of Linthal, showing: (*a*) Kilchenstock, Linthal, and the predicted area of impact; and (*b*) slope displacement measurements from which two different catastrophic failure forecasts were made, but which did not fully develop. After Löw (1997) and Heim (1932).

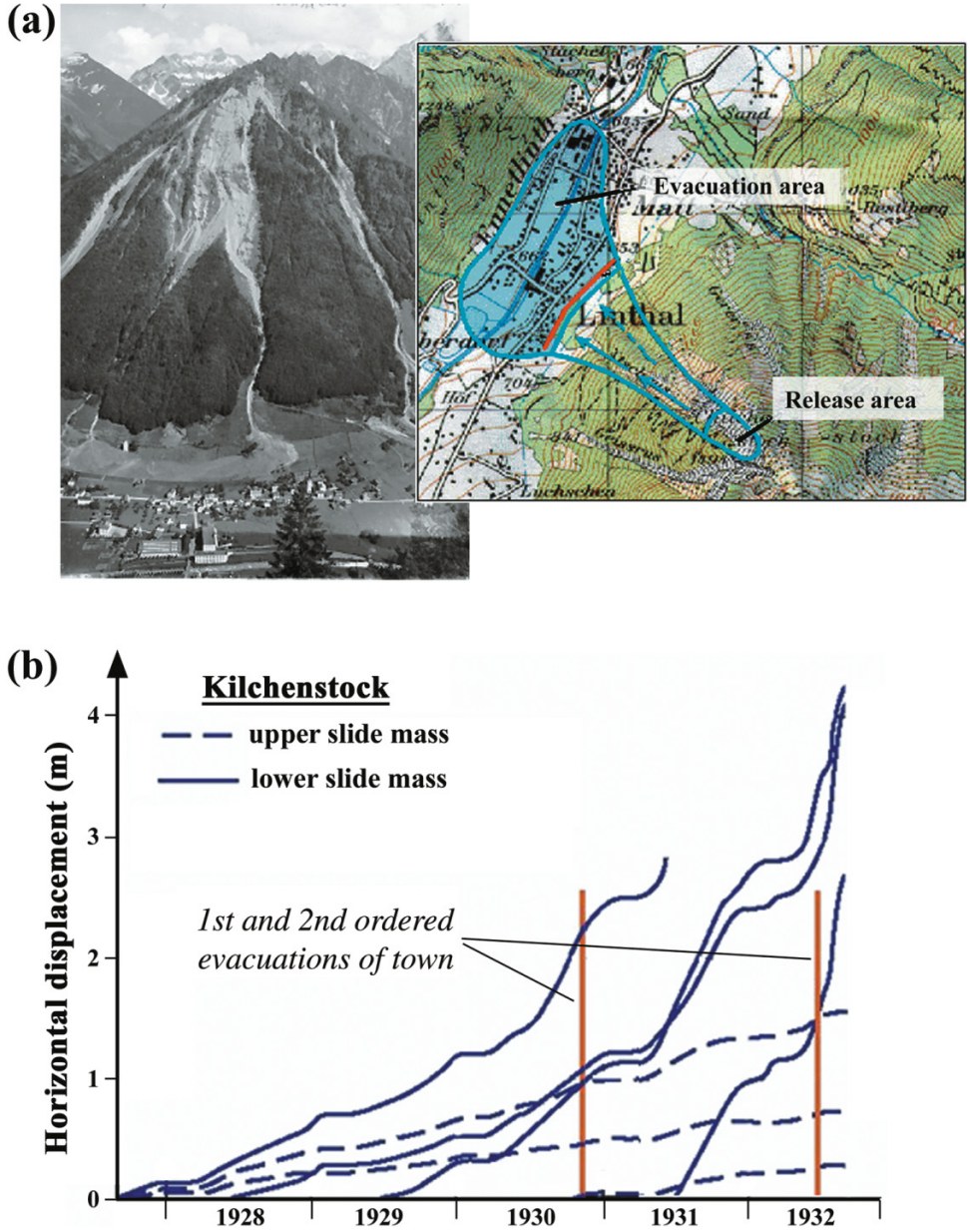

cross-cutting joints daylighting near the bottom of the working bench (Stead and Eberhardt 1997). Mapping of these features to determine their orientation is made difficult by their extremely tight nature (resulting from the large driving forces acting across the joints; e.g., Figure 12*b*), as well as by the rock fall hazard presented by the upper unbenched slope. Without an understanding of the potential mode of failure, the development of any early warning system and (or) mitigation measures would be severely limited in their effectiveness. Figure 12*c* presents the results of a series of distinct-element models showing the different modes of failure and corresponding slab displacements for three cases with varying cross-joint dip angles. The models demonstrate the complexity of these different failure modes showing that they involve both slip along the controlling discontinuities and plastic yielding of the intact rock. By closely comparing displacement vectors and trends established through geodetic monitoring of survey prisms strategically positioned across the pit wall slopes, and those derived through numerical modelling (e.g., Figure 12*c*), it becomes possible to provide real-time prognosis of the mode of failure and meaningful early warning threshold criteria. In this sense, deformation monitoring and numerical modelling are combined in accordance with Terzaghi and Peck's "observational method" (Peck 1969).

Much potential exists in how field-based data sets and numerical models are treated to limit the spatial and temporal uncertainty frequently encountered in large-scale rock slope stability problems. Rock slope deformation measurements provide an important and useful means to empirically derive

Fig. 11. Method for temporal prediction of slope failure based on inverse mean velocity as calculated from monitored surface displacements (after Fukuzono 1985).

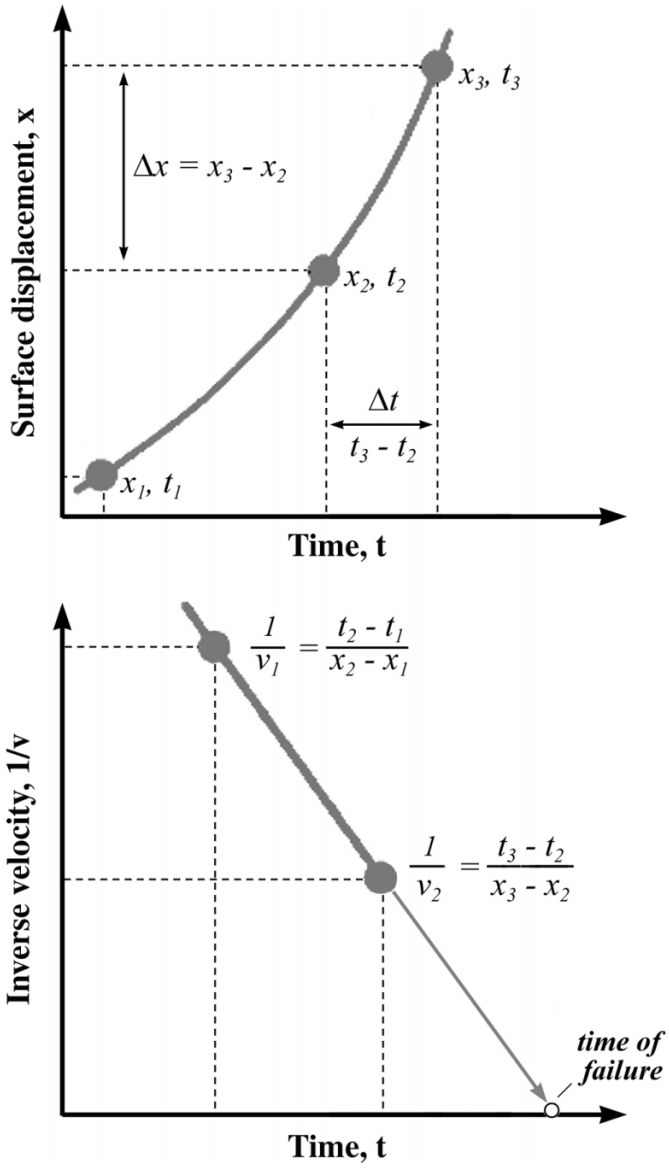

temporal predictions of failure and (or) to establish early warning thresholds, but at the same time, numerical modelling must be employed to help constrain the interpretation of complex rock slope monitoring data. Judgement must be exercised as to the prevailing external conditions involved in each individual case, including factors relating to the reliability of the monitoring network, the complexity of the displacement pattern measured, and the contributing influence of precipitation and (or) other loading conditions. In this sense, numerical modelling provides an ideal means to aid the judgment process.

Establishing slope deformation and instability mechanisms

Strength degradation, progressive failure, and internal shearing

Empirical observations tell us that an unstable rock slope may deform in a slow and ductile manner, moving continuously or intermittently, or it may fail suddenly in a brittle manner with very little warning. The difference is largely a matter of the controlling influence of geological structures and rock mass strength on the mode of failure (e.g., Fig. 1). Hungr and Evans (2004) classify rotational rock slumps, compound slides, and flexural topples as being predominantly ductile, producing slow displacements with limited displacements (i.e., self-stabilizing failure mechanisms). Brittle failures generally involve translational movements, where slope-parallel persistent structures are present (e.g., bedding planes, faults, sheet joints), or rock collapse, where no systematic structural controls are present and failure is controlled by the brittle destruction of "rock bridges" separating random discontinuities of limited persistence in stronger rock (Hungr and Evans 2004).

In June 2000, a detailed research program funded by the Swiss National Science Foundation was launched at the Swiss Federal Institute of Technology in Zurich (ETH Zurich) to investigate and study massive rock slope failures in crystalline rock (Eberhardt et al. 2001). Many of the sites studied could be classified as potential rock collapses, based on the definition of Hungr and Evans (2004). Focus was placed on brittle fracture processes and rock mass strength degradation, primarily as they contribute to deformation, shear plane development, and progressive failure of the rock slope over time. The rationale behind the research objectives was that many natural rock slopes have existed in a relatively stable state for the past several thousand years, with the last major change to their kinematic state being that of oversteepening and debuttressing–relaxation of the valley slope walls following the last glacial advance and retreat. Periodically however, one of these rock slopes will collapse, meaning that an element of time-dependent rock mass strength loss related to extensional strain, creep, fracture propagation, fatigue, stress corrosion, weathering, etc., must be present that acts to destroy intact rock bridges between nonpersistent, nonsystematic discontinuities and (or) asperities between locked joint surfaces over time (e.g., Kemeny 2003). Triggering factors, for example a heavy precipitation event, cannot be used to solely explain the occurrence of such catastrophic collapses, at least not in the traditional limit equilibrium sense of changing the balance between resisting and driving forces, as most triggering episodes rarely stand out as being exceptional when compared to those that had occurred in the past. The 1991 Randa rockslide in the southern Swiss Alps is one such example.

The 1991 Randa rockslide

The 1991 Randa rockslide (Fig. 13*a*) involved the failure of 30 million cubic metres of rock in two successive episodes, each lasting several hours, approximately 3 weeks apart (Fig. 13*b*). Failure coincided with a period of snow melt, however analysis of climatic and seismic data showed no clear indications of an exceptional triggering event (Schindler et al. 1993). Eberhardt et al. (2001) instead suggested that time-dependent mechanisms relating to rock mass strength degradation and progressive failure were the primary factors that brought the slope to failure, with snowmelt and precipitation providing the final impetus.

The failed rock mass was comprised of massive orthog-

Fig. 12. Example of dip slope failures commonly encountered in western Canadian open pit coal mines, showing: (*a*) 460 m high unbenched footwall slope dipping at 30° and steepening to 35° (Quintette coal mine, British Columbia, Canada); (*b*) tight cross-joints in footwall slope; and (*c*) distinct-element modelling of complex failure modes, showing plasticity indicators and movement vectors of driving and passive slabs.

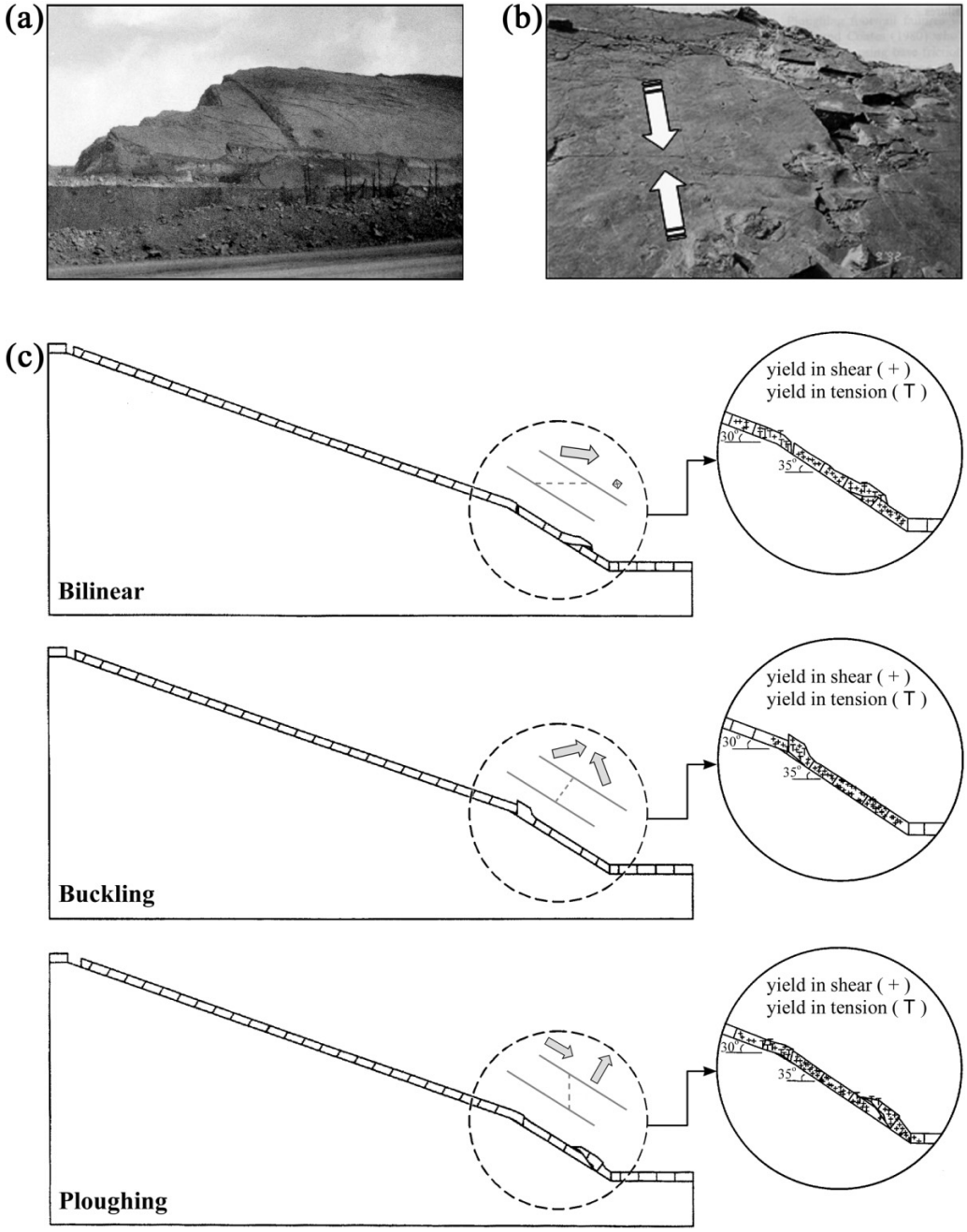

neiss units overlain by mica-rich paragneiss, with foliation dipping favourably into the slope (Figs. 13*c*). Thus in part, shear surfaces were required to cut across these planes of weakness, producing a detachment surface that was steep and irregular (Fig. 13*d*). At the base of the rock slope, Sartori et al. (2003) reported the presence of a 30° dipping basal fault zone along which the first slide block detached (18 April 1991 episode). The second rockslide event (9 May 1991; Fig. 13*b*) is reported to have slid along a 40° surface formed along highly persistent shallow-dipping joints. However, although traces of these joints appear to be visible along the exposed sliding surface, Willenberg (2004) found them to be relatively scarce in surface outcrops and borehole images. Instead, Eberhardt et al. (2004*a*) used these field observations and a series of numerical models to demonstrate that fully persistent joints were not necessary to explain the kinematics of the rockslide, but that stress- and strain-driven brittle fracture processes could also have enabled kinematic release through internal shearing and the progressive development of a basal shear surface stepping up through the rock slope.

Numerical case study of the 1991 Randa rockslide

Numerical analyses of the 1991 Randa case study show

Fig. 13. (*a*) The 1991 Randa rockslide in southern Switzerland. (*b*) Geological profile showing the outline of the two failure episodes (after Wagner 1991). (*c*) Photo showing foliation of paragneiss dipping into the slope. (*d*) Photos of steep, irregular detachment surface.

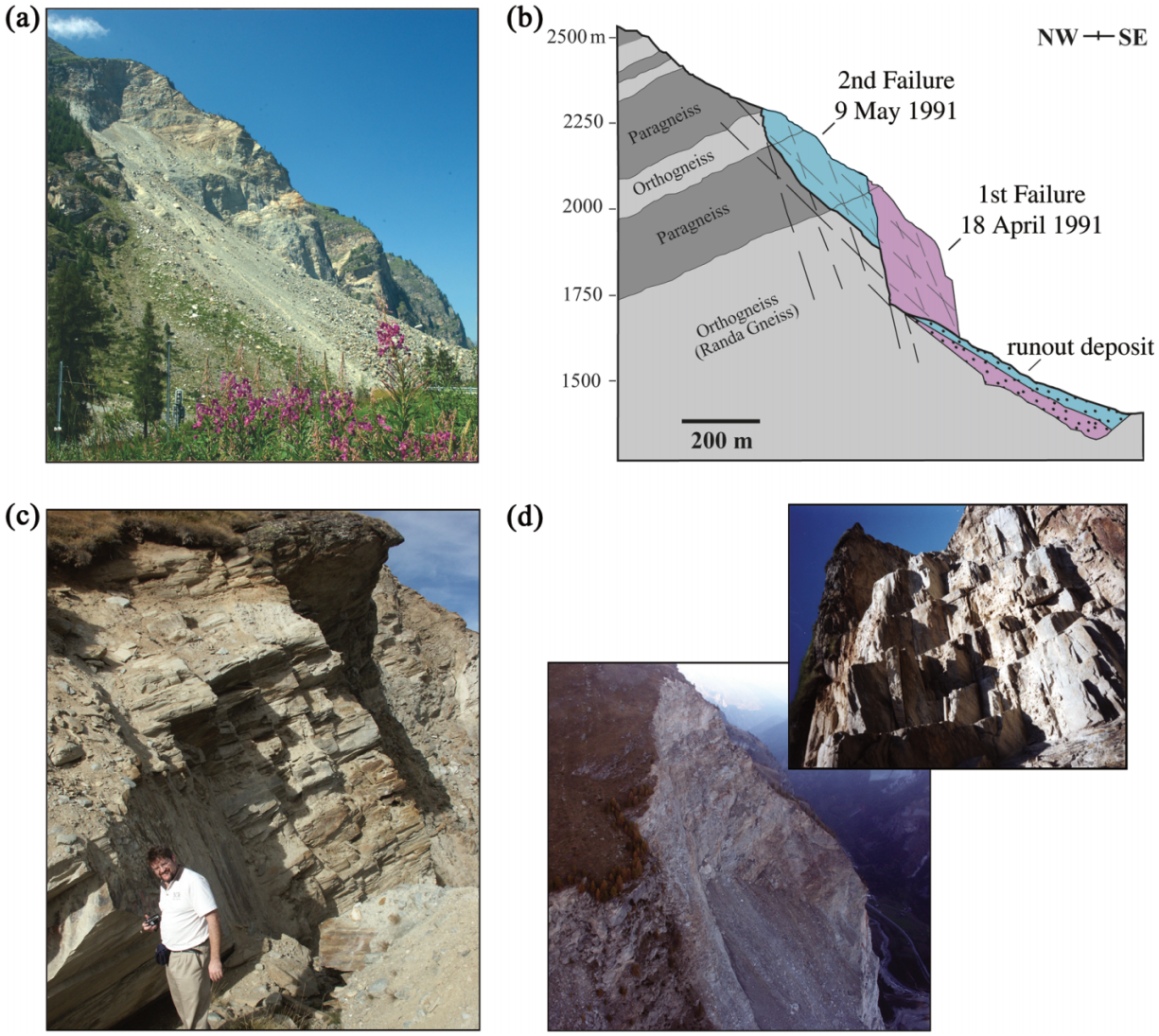

that, starting from the assumption of a continuum, the problem is one that is initially stress driven (Eberhardt et al. 2004*a*). Glacial oversteepening of the valley walls resulted in shear stress concentrations developing at the toe of the slope (Fig. 14*a*). These stress concentrations would in turn act to promote brittle fracture propagation, leading to strength degradation and yielding of the rock mass. Figure 14*b* shows the results of modelling efforts incorporating a strain softening model where the strain-dependent values of cohesion and friction were roughly estimated from acoustic emission and strain data recorded for a series of uniaxial compression tests on granite (Eberhardt et al. 1999, 2004*a*). As shown in Fig. 15, the rock mass strength was modelled as being initially cohesive, with frictional strength mobilizing as cohesion is destroyed. This follows the findings outlined by Martin (1997) for the progressive failure of brittle rock. Hajiabdolmajid and Kaiser (2002) adopted a similar strain-dependent cohesion weakening – frictional strengthening constitutive approach in modelling of the 1906 Frank slide.

The results of the Randa model show a surprisingly good agreement between the modelled yield surface and the outline of the actual failure surface, given the overly simplified 2-D continuum representation of the problem (Fig. 14*b*). It should be further noted that where the model appears to overpredict the location of the back-scarp in the upper section of the slope, the same area corresponds to the location of several present-day deep open tension cracks (Fig. 14*c*).

The opening of tension cracks at the head of the slide suggests that the latter stages of rock slope failure are more strain-controlled than stress-controlled. Modelling results support this argument, showing that the initialization of the failure process may be stress-driven (or accommodated by the stress concentration that develops at the toe of the slope), but that with yielding and strength degradation of the rock mass, the progressive development of failure is largely strain driven; the free surface and unconfined face formed by the steep slope enables down-slope extensional strains to develop as gravity pulls on the slope mass. Stacey et al. (2003) found that very large zones of extension strain can develop around deep open pit mine slopes, the magnitudes of which would likely result in the development of extension fractures. Similar modelling performed for the 1991

Fig. 14. Numerical analyses of the 1991 Randa rockslide, showing: (*a*) initial shear stress concentrations at the toe of the glacially oversteepened valley walls; (*b*) resulting shear strain contours assuming a strain softening constitutive model (see Fig. 15); (*c*) present day, deep, open tension cracks above the back scarp of the 1991 collapse events; (*d*) extension strains calculated for the prefailure geometry; and (*e*) hybrid finite – discrete-element brittle fracture model showing the progressive development of the failure surface superimposed with that of the 1991 Randa rockslide events. After Eberhardt et al. (2004*a*).

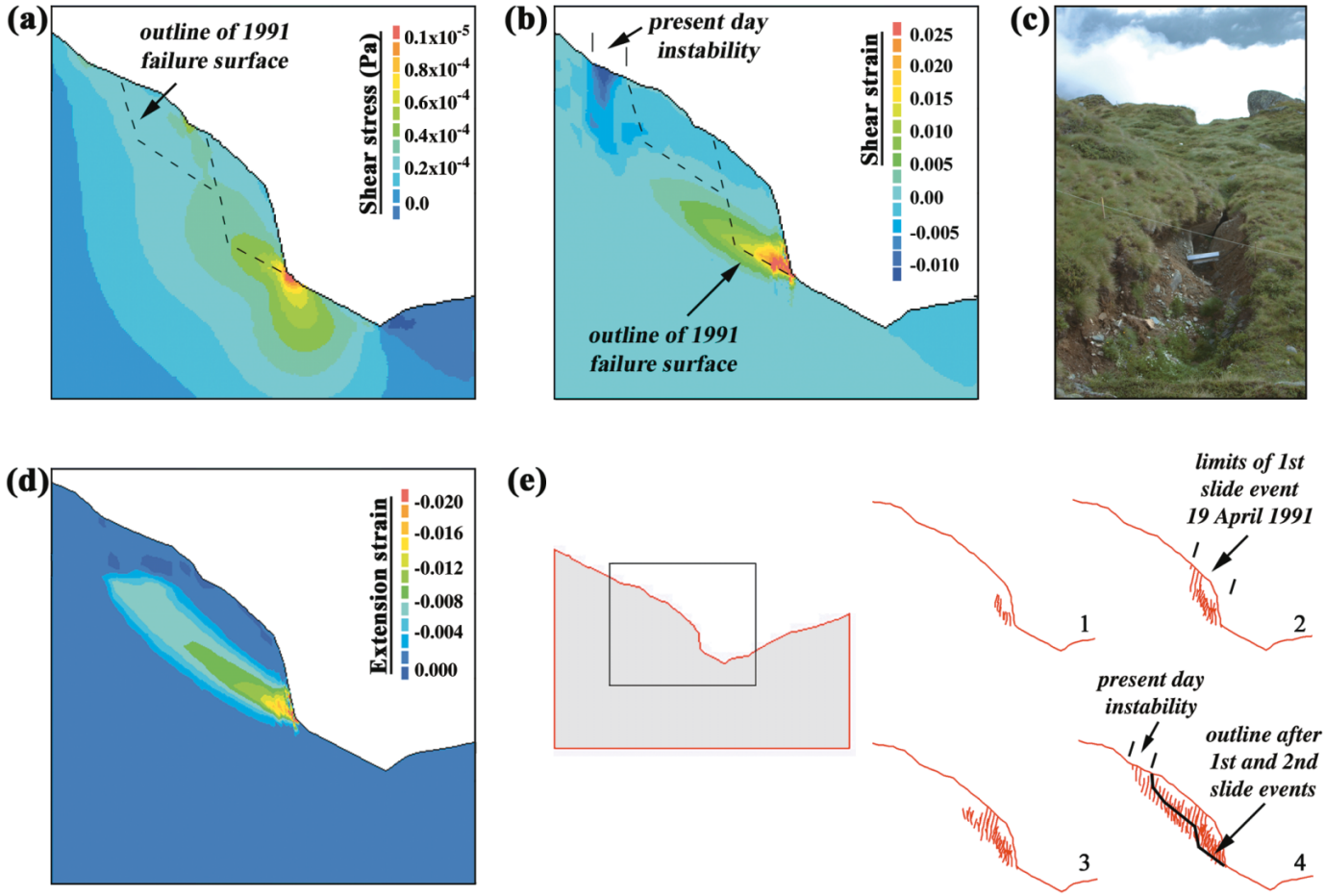

Fig. 15. Strain softening relationship used for Randa models shown in Fig. 14*b*, in which cohesion decreases and friction mobilizes as a function of increasing plastic shear strain, γ_p (i.e., increasing brittle rock mass damage). After Eberhardt et al. (1999, 2004*a*).

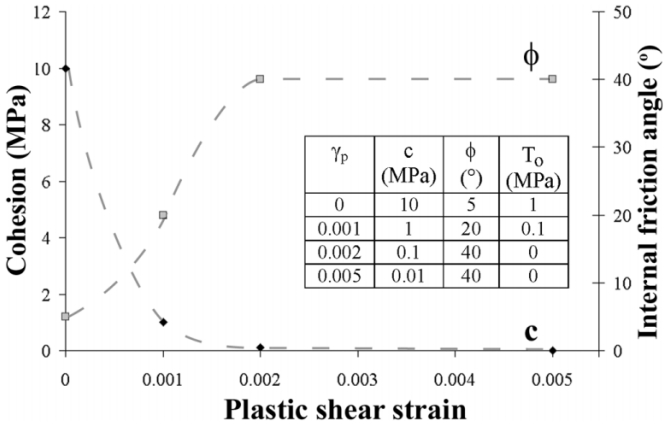

γ_p	c (MPa)	ϕ (°)	T_o (MPa)
0	10	5	1
0.001	1	20	0.1
0.002	0.1	40	0
0.005	0.01	40	0

Randa rockslide suggests that the strains produced in the model are well in excess of those reported by Stacey (1981) as being critical for brittle fracture initiation and propagation (Fig. 14*d*).

To better model these processes, Stead et al. (2006) introduced new developments in hybrid finite – discrete-element techniques, which allow for the explicit modelling of brittle fracture initiation and propagation. These techniques differ from earlier attempts to model rock slope failure through brittle fracturing using the displacement discontinuity method, a type of boundary element technique (e.g., Scavia 1995; Muller and Martel 2000). Although the latter are more computationally efficient, as only the boundaries of the cracks are required to be updated during propagation and not the problem domain surrounding the cracks, the solutions rely on the assumption of an elastic medium. As a result, the boundary element treatment of the fracture criteria, based on linear elastic fracture mechanics, is largely stress driven and therefore more limited when it comes to properly simulating the latter stages of failure development, which appear to be more strain controlled. The simulation of plastic softening and damage leading to brittle fracturing requires discretization of the problem domain, as is done when using finite-element solutions. Hybrid finite – discrete-element techniques build on this by using discrete elements to represent the interactions (i.e., opening, closing, and (or) shear) along existing or newly developed fractures, together with

Fig. 16. Empirical prediction of time to failure for the second Randa rock slide event (9 May 1991) based on geodetic data collected following the first Randa collapse event on 18 April 1991 and Fukuzono's (1985) inverse velocity method. Data source: Ischi et al. (1991).

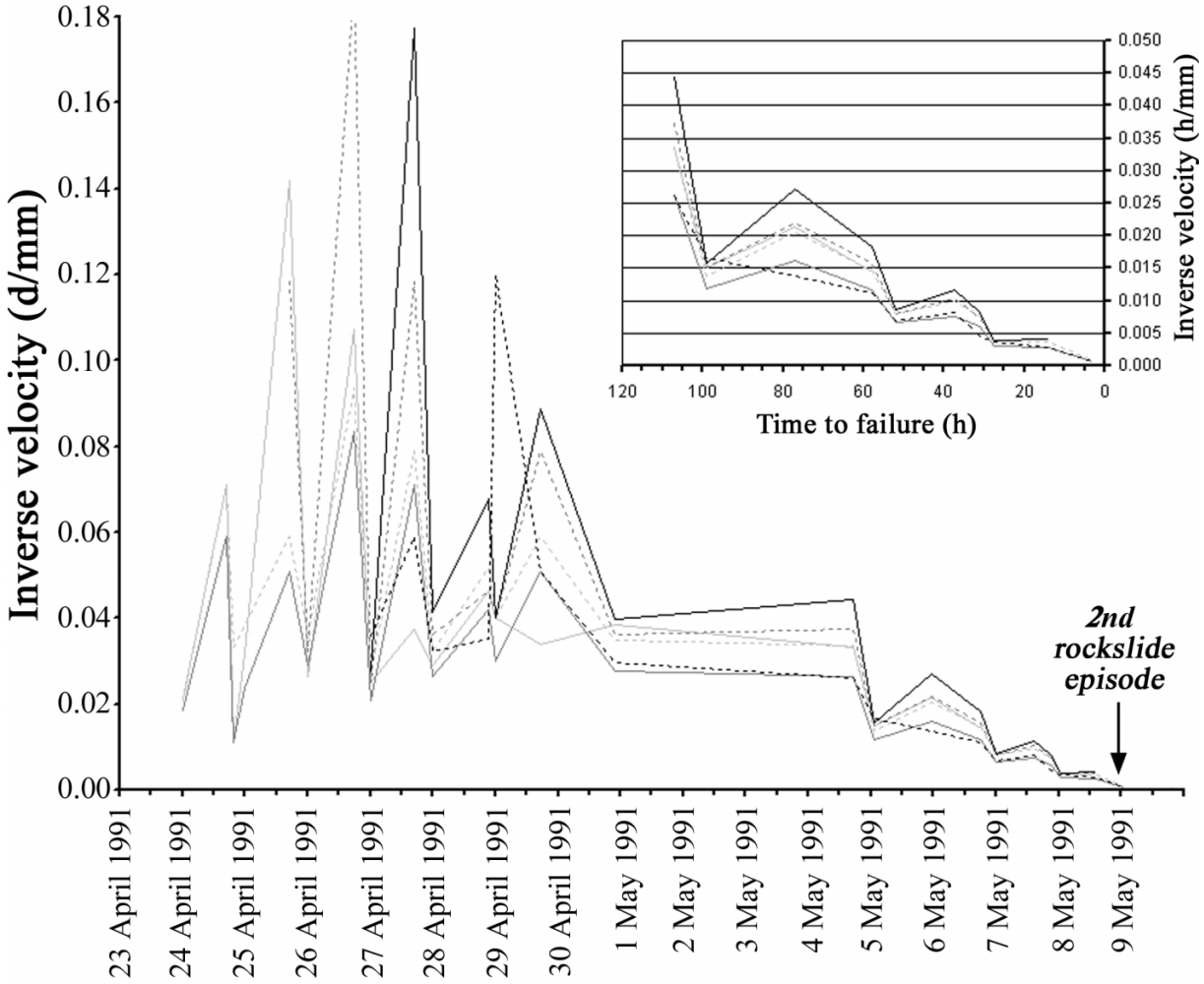

adaptive remeshing, contact search algorithms, and a fracture energy approach controlled by a designated constitutive fracture criterion to simulate the progressive development of a brittle fracture system (Munjiza et al. 1995).

The results in Fig. 14*e* show the initiation and propagation of a brittle fracture system for the 1991 Randa rockslide, starting from that of an initial continuum based on the original topography. A Mohr–Coulomb based constitutive model with a Rankine tensile cut-off was used, through which the stress-induced extensional plastic strains are coupled to the degradation of tensile strength to explicitly model discrete brittle fracturing.

Through these results, the role of extensional strain in rock mass strength degradation and progressive failure is more effectively captured; the extensional strains and elastoplastic yielding induced through the downslope movements of the continuum result in the initiation and propagation of numerous subvertical fractures (i.e., normal to the direction of downslope strains). As the density of these fractures increases, the shear plane progressively steps up and through, developing perpendicular to the extension fractures and forming a curvilinear failure surface. Although not explicitly included, the presence of any low-angled dipping natural joints would further serve to aid the failure process, aligning to form a stepped shear plane that could accommodate further movements and kinematic release of the slide mass.

In addition to modelling the irregular outline of the failure surface, these hybrid models were also able to reproduce the staged nature of the failure by first simulating the development of the 18 April 1991 Randa rockslide event, followed by the 9 May 1991 event (Fig. 14*e*; 1 to 4). The ability to model the progressive nature of a massive rock slope failure provides the potential to constrain hazard assessments and runout predictions with respect to the degree of internal shearing and coherency involved in the failed slope mass. If the moving mass fails coherently, higher velocities may accompany failure, whereas if the moving mass is ruptured internally and slowly disintegrates (failing block by block) the travel distance and area covered would be much more limited. This was used by Eberhardt et al. (2004*a*) to explain the anomalously short runout distances attributed to the Randa rockslide events when compared to other rockslides of similar volumes as compiled by Scheidegger (1973).

The Randa In Situ Rockslide Laboratory – The integration of innovative geotechnical field measurements

To fully utilize the advances made in numerical modelling capabilities, especially those relating to the ability to

Fig. 17. (*a*) Layout of the Randa instrumentation network showing the location of deep boreholes and geophones relative to open surface tension cracks and the already existing geodetic monitoring network. (*b*) Seismic network geophone distribution and corresponding Dirichlet spreads for vertical cross section through X–X′ (after Spillmann 2007). Values near zero (i.e., bright areas) indicate zones of optimal resolution.

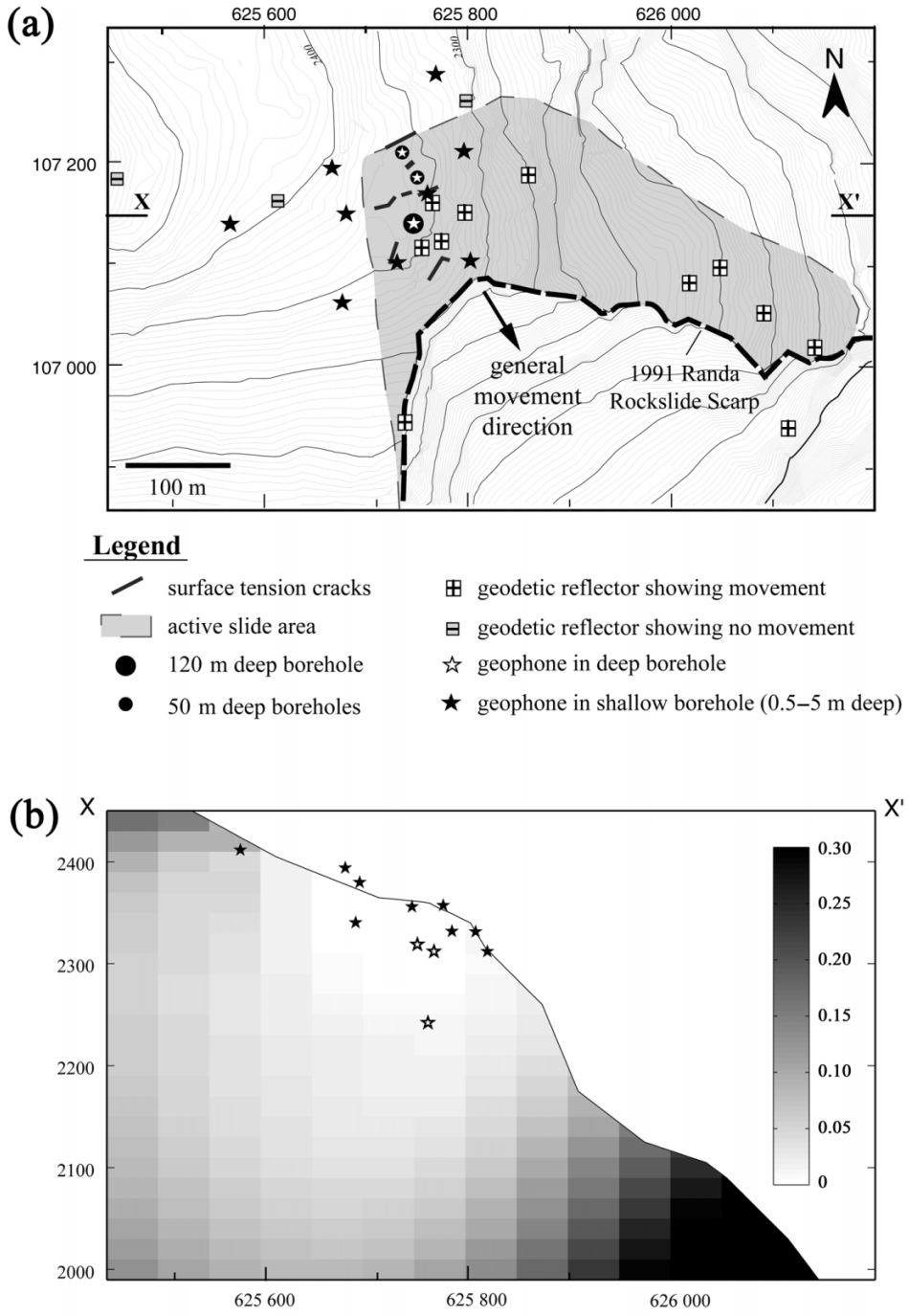

model strength degradation, brittle fracture, and progressive failure processes, similar advances must be made in field characterization and in situ monitoring techniques. Moreover, Eberhardt and Willenberg (2005) emphasize that slope monitoring should not be treated separately from the analysis phase of the rock slope hazard investigation, with the sole objective of providing data to constrain numerical models, but should be made in parallel enabling modelling to be used to help constrain the interpretation of monitoring data. For example, Fig. 16 shows the inverse velocity plot based on geodetic data collected at Randa following the first collapse event on 18 April 1991. Using Fukuzono's (1985) empirical approach, a very accurate prediction of the time of failure for the second rockslide event on 9 May 1991 is obtained, almost down to the exact hour (see Fig. 16 inset). In truth though, the accuracy of this temporal prediction is not evident unless the entire dataset leading up to failure is viewed. In real time, a correct prediction may have been possible several hours prior to failure. Yet at the same time, any one of a number of accelerations recorded in the 2 week

Fig. 18. Photos of the construction of the Randa rockslide laboratory, showing: (*a*) Super Puma helicopter transport for borehole drill rig; (*b*) drill rig atop the Randa rockslide area; (*c*) borehole instrumentation installation; (*d*) surface crackmeter and geophone installed across an active tension crack; and (*e*) instrumentation hut with solar panels and batteries for power supply.

period beforehand would likely have produced a similar, but false, prediction.

To measure processes relating to the progressive development of internal and basal rock slope shear surfaces, and improve the capabilities of established early warning methodologies, the June 2000 multidisciplinary study launched by the ETH Zurich also included plans for the construction of a first of its kind "in situ rockslide laboratory". The facility–network would integrate a variety of instrumentation systems designed to measure temporal and 3-D spatial relationships among fracture systems, displacements, pore pressures, and microseismicity. The Randa site was chosen following a preliminary investigation of several sites across the Swiss Alps (Eberhardt et al. 2001), based on the presence of ongoing movements (approximately 1–2 cm/year) above the 1991 slide scarp, the massive crystalline nature of the rock mass, the availability of geodetic monitoring data dating back to the 1991 failure, and the fact that observations relating to the earlier rockslide could be used to provide understanding of the current instability. An additional consideration with respect to the planned microseismic monitoring was the remote nature of the site and the relatively low background noise level related to heavy vehicle traffic.

Design and installation of the Randa network

The estimated volume of the active slide mass above Randa is on the order of 2–10 million cubic metres. The monitoring network design called for three deep boreholes to be drilled to depths of 120, 50, and 50 m. The locations of these boreholes (Fig. 17*a*) were chosen based on the engineering geological model developed by Willenberg (2004), as well as constraints imposed by drilling logistics, surface topography, and spatial requirements for active crosshole seismic and radar experiments. The design of the boreholes was modularized using 3 m lengths of 71 mm diameter PVC inclinometer casing to simplify installation and minimize the required diameter of the downhole assembly (including grouting tubes). Design simplification where possible was deemed necessary given the potential for difficult ground conditions leading to borehole stability issues and the remote nature of the construction site, which required helicopter transport to move equipment (Fig. 18). In the case of the drill rig and compressor, a twin-engine Super Puma helicopter was required.

The modularized borehole assembly included the packing of a vibrating wire piezometer (Geokon 4500) in a sand filter within the bottommost segment of the inclinometer cas-

Fig. 19. Borehole design used for instrumenting and completing the 120 m deep borehole at the Randa In Situ Rockslide Laboratory. The same design was followed for two 50 m deep boreholes, but without the in-place inclinometer and INCREX extensometer.

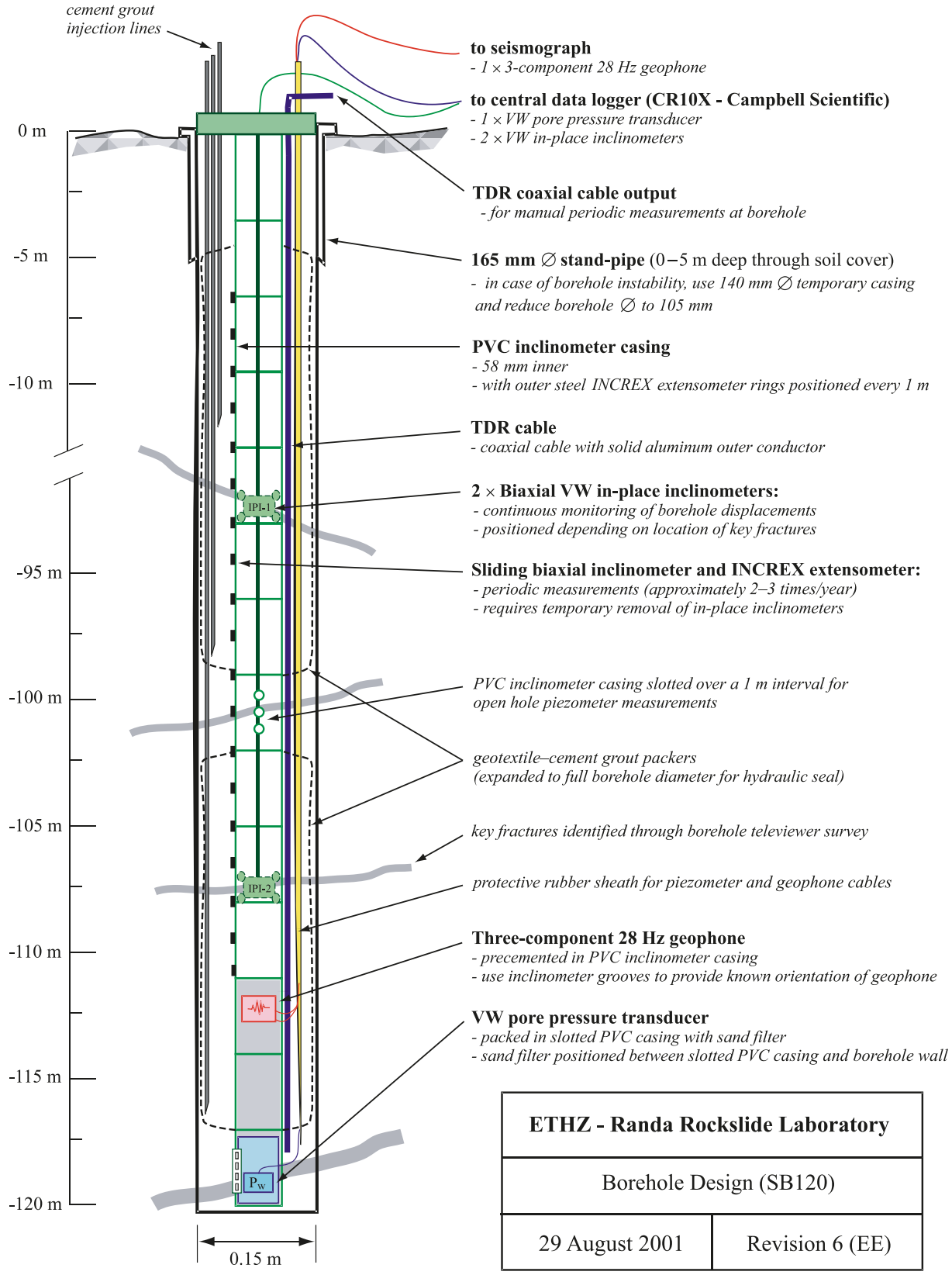

Fig. 20. Schematic diagram of the Randa instrumentation network and data acquisition system (after Willenberg 2004).

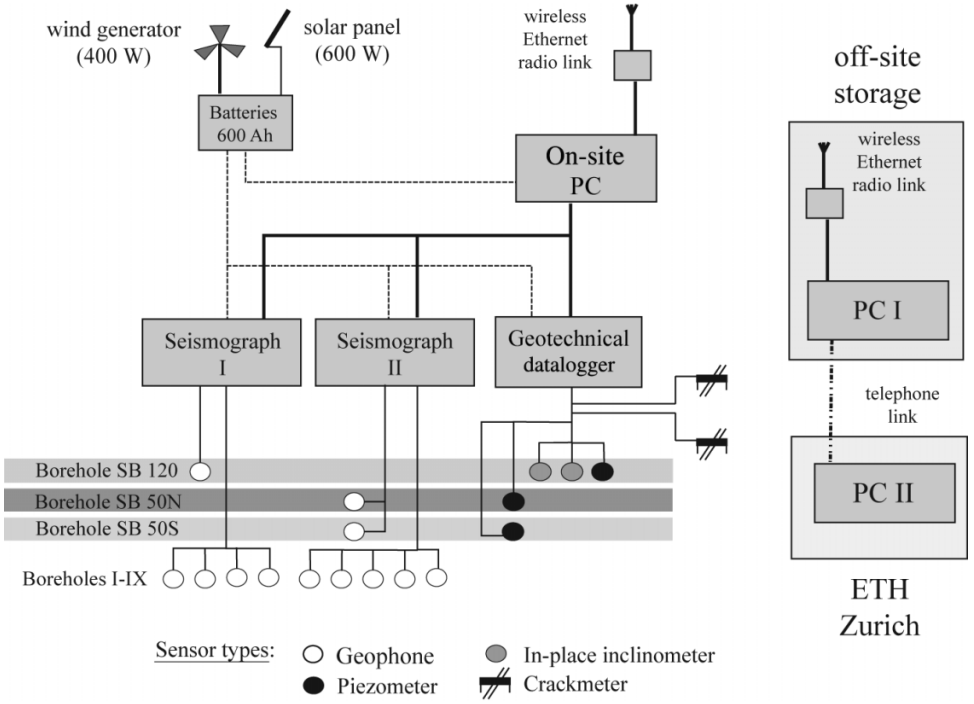

ing, with slots cut into the PVC to allow groundwater to equilibrate with the sensor. This was followed by a 3 m segment used to aid in packing off the piezometer interval and a 3 m segment housing a three-component, 28 Hz geophone cemented within it (Fig. 19). By pre-installing these devices within the casing, it was possible to position and pack off the piezometer modules along zones showing significant fracture permeability as determined from borehole televiewer data. The use of the inclinometer casing to mount the geophones, which were fixed relative to the biaxial inclinometer grooves, enabled the orientation of each geophone's horizontal components to be established. The remaining inclinometer segments above the geophone were left open for normal inclinometer use.

Outside the inclinometer casing, brass rings were fixed at 1 m intervals to enable the use of an electromagnetic induction sliding extensometer (Interfels' Increx system), and a 12.7 mm diameter solid aluminum coaxial cable (CommScope P3 500 CA) was attached for time domain reflectometry (TDR) measurements. The TDR cable was included as a low-cost backup to the inclinometer in case later deformations prevented passage of the inclinometer tool (O'Connor and Dowding 1999). The entire borehole package was then enclosed in a geotextile sock to help in lowering the casing and various cables and grouting tubes down the borehole without cutting or damaging them against the rough borehole walls (Fig. 18*c*). The geotextile was then filled with cement grout to fix the inclinometer and TDR cable in place, as well as to pack off the designated piezometer intervals.

The boreholes were completed with lightning protection, and in the case of the 120 m deep borehole, a vibrating wire in-place inclinometer (Geokon 6300) was lowered into place with inclinometer heads positioned at depth intervals coinciding with key fractures identified through earlier borehole televiewer surveys. The biaxial in-place inclinometers served to provide continuous monitoring of subsurface deformations along these structures, but could be removed for periodic inclinometer- or extensometer-probe measurements along the entire borehole length (to be performed two to three times per year).

On the surface, the network included the addition of two vibrating wire crackmeters (Geokon 4420) positioned across two open tension cracks for continuous monitoring (Fig. 18*d*). These measurements were supplemented with periodic measurements made by hand across other open tension cracks and the already existing network of geodetic reflectors (Willenberg 2004). To the three deep borehole geophones were added nine 3-component, 8 Hz geophones in shallow boreholes 0.5–5 m deep (Fig. 17*a*). The spatial distribution of these sensors was chosen such that the array's resolution was concentrated to the active sliding area (Fig. 17*b*). This ensured that the hypocentre parameters generated from the seismic sources could be reliably constrained within the area of interest (Spillmann 2007).

Seismic activity recorded by the 12 geophones was monitored using two 24-channel seismographs. A parallel system was used to automatically record borehole piezometer, in-place inclinometer, and crackmeter measurements (Fig. 20). These instruments were sampled every 6 min and stored on a Campbell Scientific CR-10X data logger. Through a dial-up connection, the measurement values were directly accessed and downloaded using a local network connection. The volume of data produced by the microseismic system (on the order of 1–2 Gbytes/day) required that the on-site storage computer be linked to a central recording location in the valley below through a wireless Ethernet connection (Fig. 20). This concept also enabled access to the seismic data files and allowed for the recording parameters to be ad-

Fig. 21. Integrated borehole data set for the 120 m deep borehole at Randa, showing from left to right: fracture frequency log, optical televiewer log (highlighting traces of major fractures), cumulative inclination changes for a 2 year period (and corresponding kinematic interpretation), cumulative axial displacements for the same 2 year period, and corresponding 3-D displacement vector magnitudes and orientations (after Willenberg 2004).

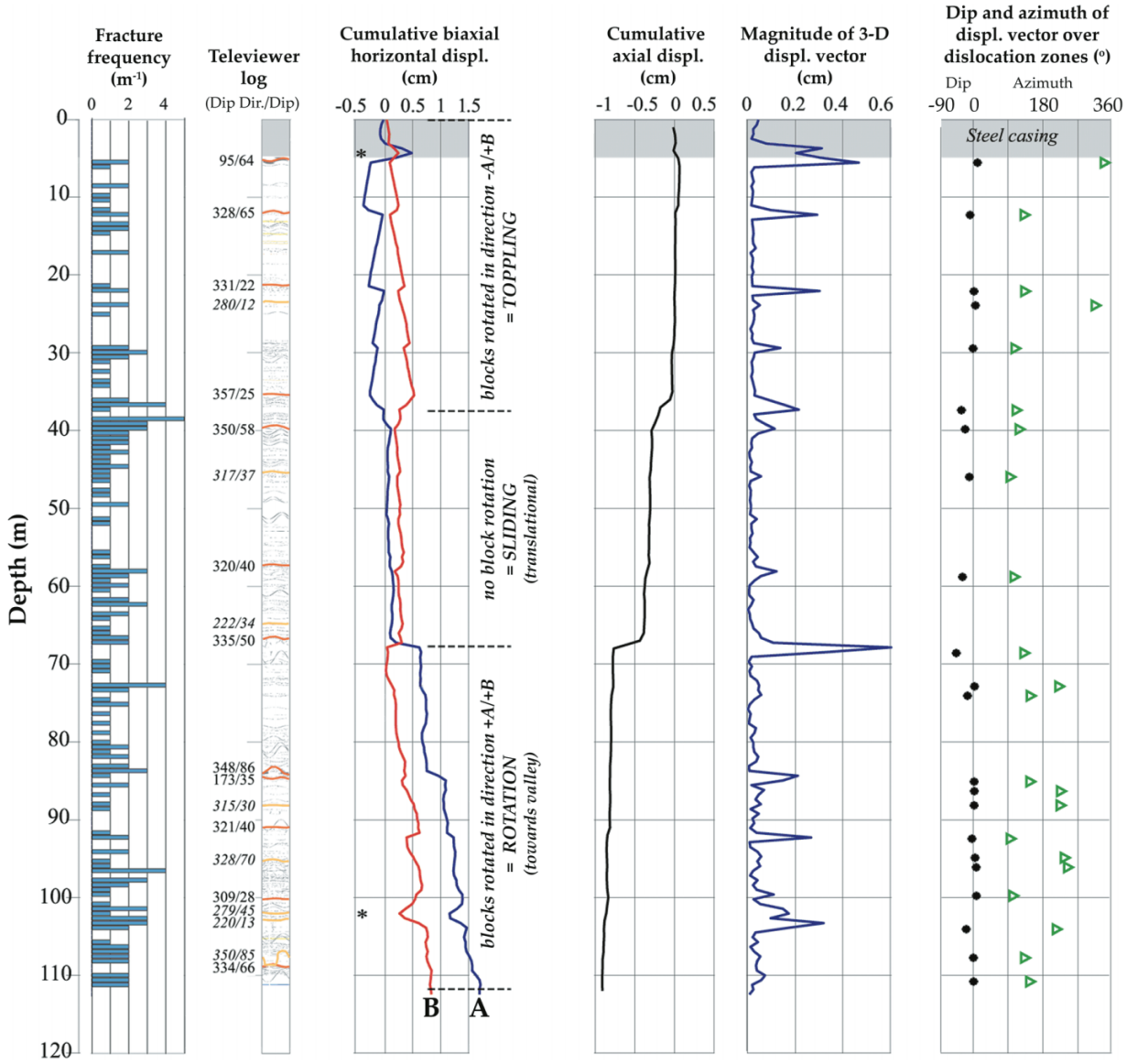

justed remotely. Solar panels combined with a wind generator were used to supply the necessary power on site (Fig. 18*e*; Fig. 20).

Integration of rock mass characterization and monitoring data with numerical modelling

The instrumentation network at Randa formed but one component of the long-term multidisciplinary study carried out through the rockslide laboratory, with other components involving geological and borehole televiewer mapping, 3-D surface georadar and seismics, crosshole georadar and seismic tomography (using the three deep boreholes drilled), plus the numerical modelling already described herein. The 3-D surface seismic refraction and georadar surveys focused on the use of these techniques to resolve subsurface 3-D fracture distributions. This work was completed as part of a doctoral thesis study by Dr. Björn Heincke at the ETH Zurich (Heincke 2005) and included the development of methodologies to account for rugged topography and to emphasize steeply dipping fractures. The borehole radar and crosshole seismic experiments, together with the analysis of the microseismic data, were carried out as part of the doctoral thesis study of Dr. Tom Spillmann, ETH Zurich (Spillmann 2007). The geological features identified through the geophysical surveys were compared to those mapped on the surface and in the boreholes (Fig. 21), using an optical televiewer, to develop a 3-D geological model of the unstable rock mass. This analysis, and that of the geotechnical data, was the subject of the ETH Zurich doctoral thesis study by Dr. Heike Willenberg (Willenberg 2004). A detailed accounting of the results of the Randa field investigation is reported in Willenberg et al. (2008*a*).

To this was added the inclinometer data, which required a

Fig. 22. Distinct-element modelling of complex rock slope displacements at Randa and comparison between measured and modelled cumulative displacement profiles for a step-path mode of instability, assuming: (*a*) an elastic constitutive model for the intact block deformation (after Willenberg 2004); and (*b*) an elastoplastic constitutive model for the intact block deformation. Note that model boundaries extend beyond those shown.

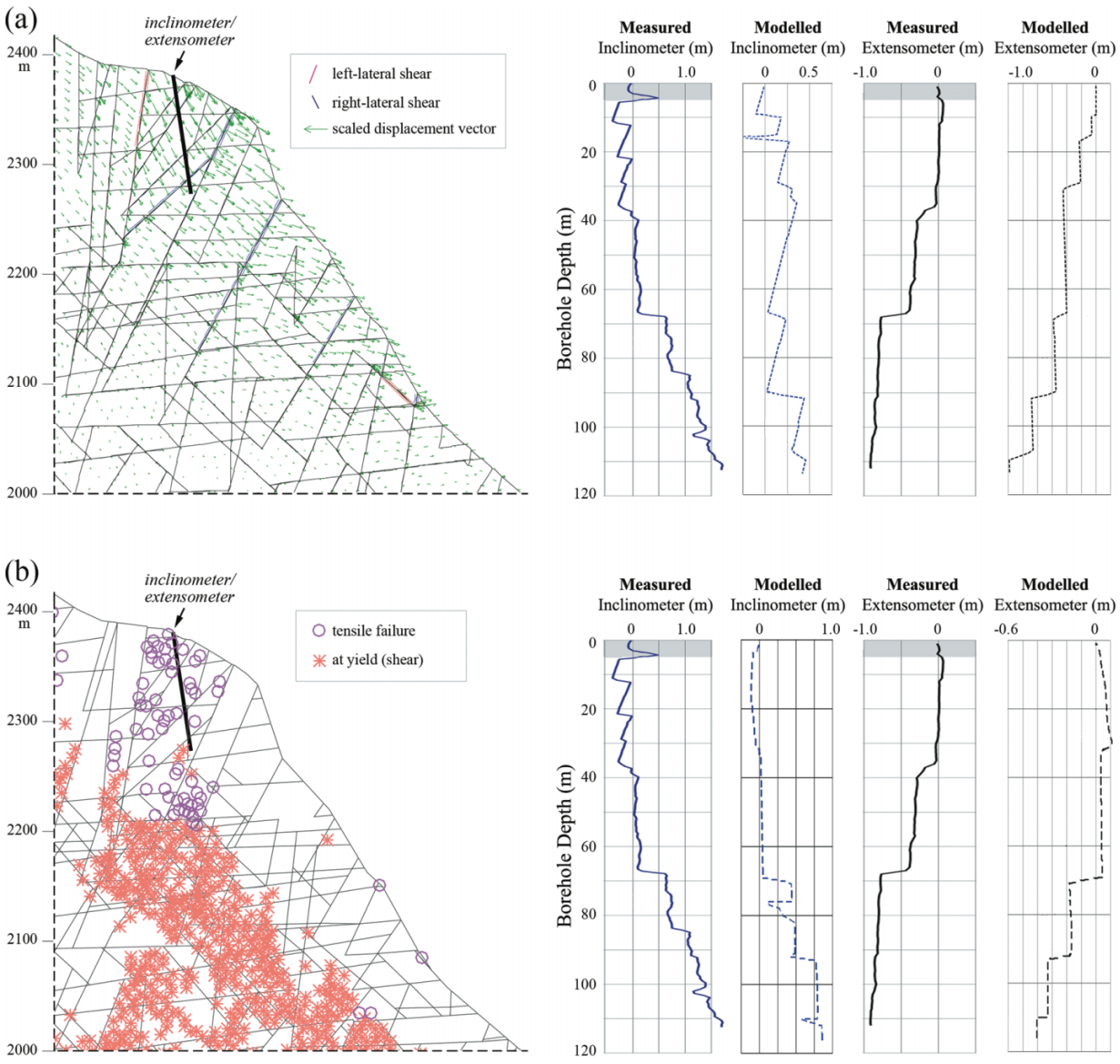

set of detailed correction factors to localize and resolve the relatively small displacements acting across the different fractures mapped along the boreholes (Fig. 21). These corrections included those to account for torsion of the biaxial grooves with depth, nonverticality and contortion of the casing, and small centimetre-scale mismatches in the depth scales of the different repeat inclinometer surveys (Willenberg et al. 2003, 2008*b*). One finding of the detailed analysis performed (Willenberg et al. 2008*b*), was that contrary to the projections derived from the initial site investigation, the combined surface and borehole displacement data suggested that the bottom of the 120 m deep borehole did not reach stable rock and was rotating outwards towards the valley (as shown in Fig. 21). Numerical modelling was therefore used by Willenberg (2004) to identify and constrain possible sliding surface scenarios that would produce displacement patterns similar to those measured in situ. These included toppling movements in the upper 35 m of the borehole, translational sliding between 35 and 70 m, and outward rotation towards the valley below 70 m to the borehole bottom at 120 m (Fig. 21).

For this, Willenberg (2004) generated several distinct element (UDEC) models, which explicitly included the key active geological structures identified through surface and borehole mapping, but differing in terms of the nature of the rupture surface and therefore mode of failure (e.g., rotational, bilinear, step-path, etc.). Direct comparisons were made between measured inclinometer and extensometer readings and those modelled using a simulated inclinometer–extensometer in the model. Based on the different failure mode scenarios,

Fig. 23. Distinct-element modelling of complex rock slope displacements at Randa showing the development of a deep-seated shear surface.

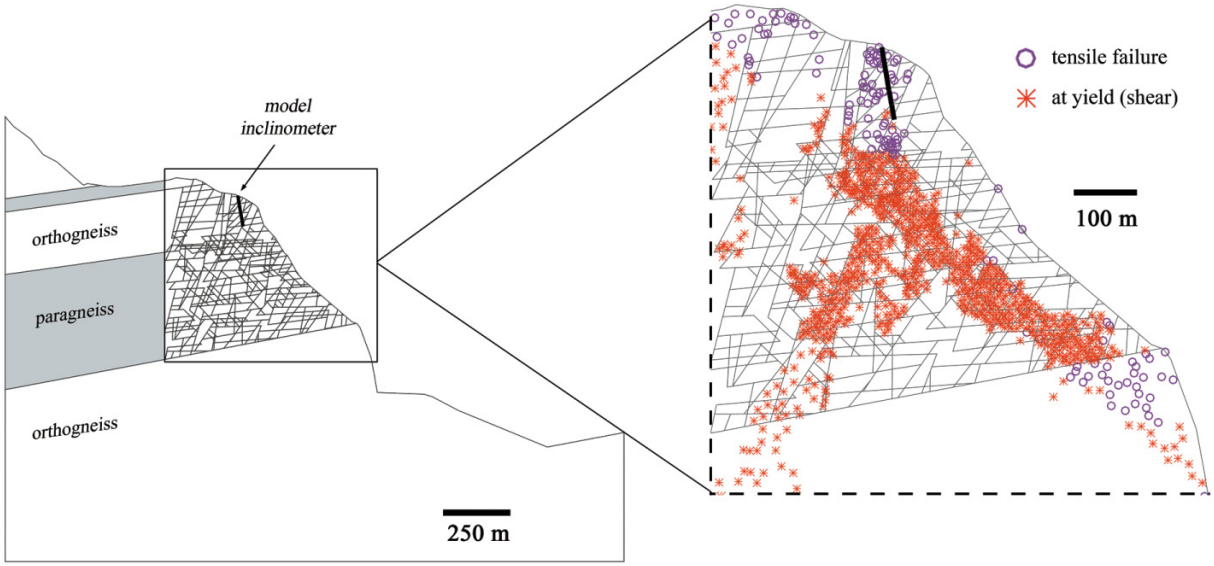

Willenberg (2004) found that the step-path mode of failure best reproduced the measured deformation patterns and mapping observations (Fig. 22*a*).

The scope of Willenberg's (2004) work, however, only focused on linear elastic constitutive models for the intact block deformations. As previously noted for the analysis of the 1991 rockslide at Randa, Eberhardt et al. (2004*a*) showed that strength degradation and plastic yield enabling internal shearing and the progressive development of a basal shear surface were key to modelling the failure kinematics. Figure 23 shows the results of the same step-path model used by Willenberg but incorporating a Mohr–Coulomb elastoplastic constitutive model for the intact rock blocks. Strength properties were varied between the mapped orthogneiss and paragneiss intervals based on rock mass characterization exercises that suggest that the orthogneiss is stronger than the paragneiss. Properties were scaled to those for an equivalent continuum to account for smaller scale discontinuities not explicitly included in the distinct-element model; c = 1.0 MPa, $\phi = 40^\circ$, and T_o = 0.5 MPa for the orthogneiss, c = 0.5 MPa, $\phi = 30^\circ$, and T_o = 0.25 MPa for the paragneiss. Results from this model show that a better fit is achieved between the measured and modelled inclinometer and extensometer deformations (Fig. 22*b*). Specifically, the model shows the same toppling movements in the upper 30 m of the borehole, translational sliding in the middle, and outward rotation towards the valley below 70 m as observed in the inclinometer and extensometer measurements. These results suggest that deep-seated yield (Fig. 23) accounts for the outward rotation of the lower intervals of the rock mass, while the explicit inclusion of discontinuities mapped in the borehole captures several complex block motions controlled by movements along persistent fractures.

In time, it is hoped that the integration of the microseismic data from Randa may also be able to provide key insights and further constraints as to the depth and contributing role of shear slip and strength degradation to the progressive development of the instability. Initial work with the microseismic system (Spillmann 2007) concentrated on overcoming challenges imposed by an unknown noise source that resulted in the frequent triggering of the system following its installation in 2001. These high frequency "noise bursts" generated exceptionally large volumes of data (>500 Gbytes), requiring the testing of smaller data sets to improve event detection and develop efficient data processing routines. The processing of these smaller data sets has confirmed that the slope mass is microseismically active (e.g., Figure 24*a*) and that numerous large open fractures are present deep below the surface across which passing seismic waves are strongly attenuated. Figure 24*b* shows the vertical component of a recorded event detected by all 12 geophones, sorted according to the source–receiver distance (A1 being the farthest from the source and B5 the closest). With the exception of B5, harmonic signals with dominant frequencies of 20 Hz and emergent first breaks characterize the seismograms. When applying a 100/500 Hz bandpass filter, the frequency range expected for brittle fracture-induced microseismic events (i.e., higher frequency), only the closest sensor B5 (21 m away from the source) was able to record significant amplitudes above 100 Hz. The high frequency information is strongly attenuated for the remaining sensors with source–receiver offsets between 40 and 200 m (Eberhardt et al. 2004*b*). Larger low frequency events, such as those generated from natural seismic activity in the region, do not suffer as much from signal quality degradation. These findings point to the presence of large open fractures deep below the surface, an observation that is in agreement with the geological model developed by Willenberg et al. (2008*a*). Based on these results, new processing algorithms must be devised that are capable of extracting more information from the microseismic data with respect to the subsurface deformation processes (Spillmann 2007).

Conclusions

Issues related to geological complexity and uncertainty represent a significant obstacle to better predicting the spatial and temporal evolution of catastrophic rock slope failures. The findings summarized in this paper emphasize the

Fig. 24. (*a*) Map view and cross section of the Randa microseismic geophone array showing the location of a recorded event. (*b*) Vertical components of the located event showing the raw (left) and 100–500 Hz bandpass filtered (right) signals. Signals are sorted according to the source–receiver distance, with sensor A1 being the farthest and B5 the closest. Absolute time scale is arbitrary. After Spillmann (2007).

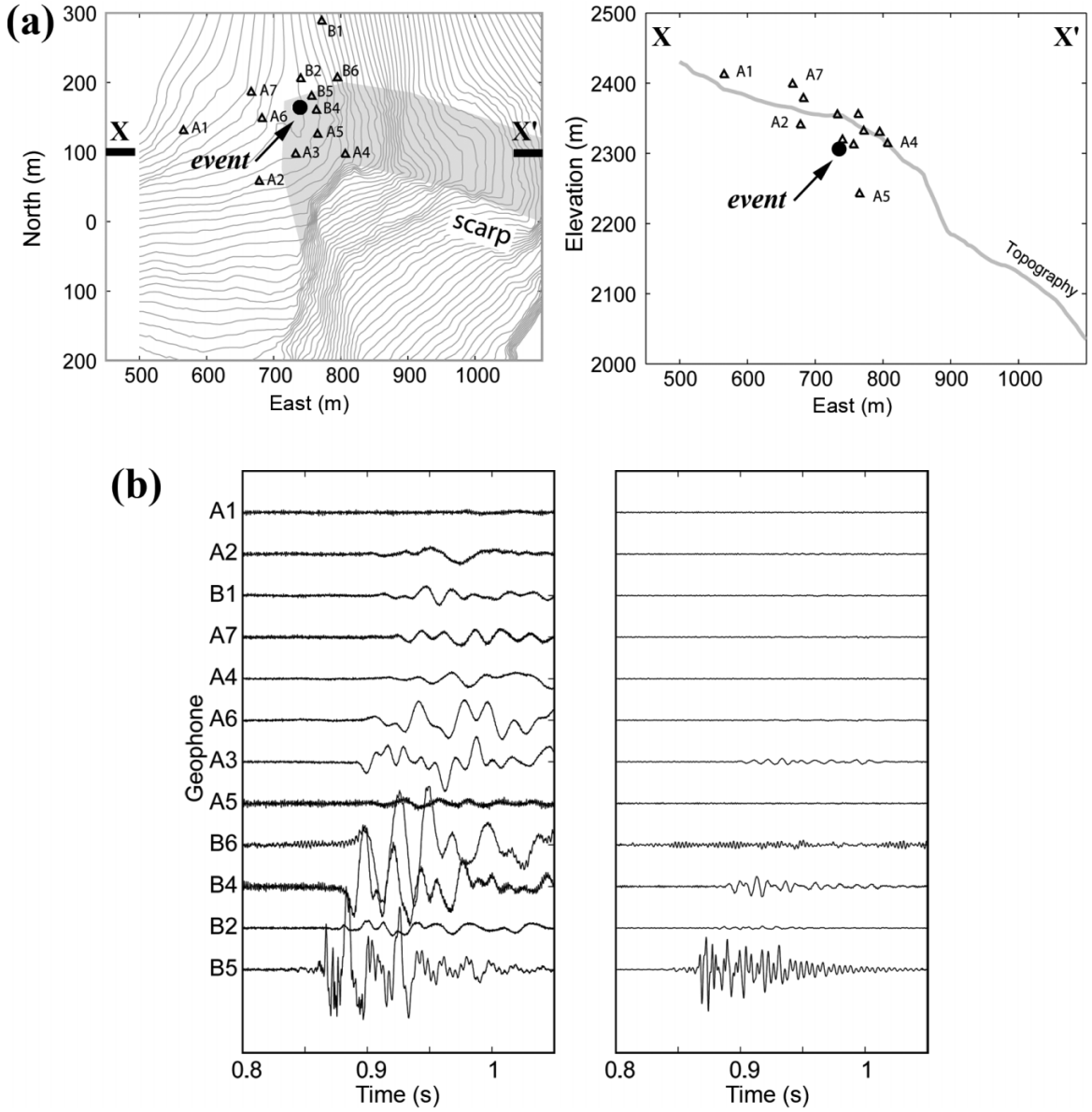

need to better integrate the various data sets collected through both field-based investigations and analytical–numerical modelling studies to overcome these challenges and bring better understanding of the controlling slope destabilizing mechanisms into the engineering decision-making process.

Several examples were presented demonstrating recent advances in the development of tools and methodologies to aid both spatial prediction (e.g., volume of potential failure) and temporal prediction (e.g., failure kinematics). For most cases, it is argued that these tools should be used in combination with one another to offset individual limitations and to link into a "total slope analysis" approach. The degree to which these tools are effective, especially when used alone, is questionable where limited consideration is given to the subsurface processes and mechanisms controlling the kinematics and evolution of the instability.

Special focus was given to deep-seated massive rock slope collapses in crystalline rock. Numerical modelling results based on the 1991 Randa rockslide events in southern Switzerland demonstrated that to explain and better predict the temporal evolution of massive rock slope failure in the absence of fully persistent controlling structures, subsurface processes involving rock mass strength degradation and progressive failure must be considered. Model results suggest that the failure process initially begins as a stress-controlled problem driven by fracture initiation and strength degradation in areas of shear stress concentration, for example those resulting from oversteepening of the slopes during glacial advance and relaxation during glacial retreat. The destabilizing process then evolves into one of strain-control, where brittle tensile fractures driven by extensional strain interact with natural pre-existing discontinuities to eventually form

basal and internal shear surfaces, which can accommodate larger displacements. Mobilization of the rock slide mass then becomes possible once the rock mass cohesion has significantly degraded and persistent shear surfaces have coalesced and evolved.

By understanding these processes, much can be gained from field-based studies that focus on brittle fracture indicators. On surface or in boreholes, these may take the form of open fractures that can be measured with respect to opening rates and displacements. At depth, over large volumes, passive monitoring of microseismic activity offers a means to detect subsurface tensile fracturing and (or) shear slip along internal fracture planes that may provide insights into the evolution of a progressively developing rock slope failure. The Randa In Situ Rockslide Laboratory in the Swiss Alps was conceived, designed, and constructed to improve our understanding of such processes, combining geological and geophysical field investigations, geotechnical instrumentation systems, and advanced numerical modelling to study mechanisms controlling prefailure rock mass deformations in massive crystalline rock slopes. Similar systems have since been developed duplicating elements of the Randa "laboratory" experiment at Turtle Mountain above the Frank Slide in Alberta, Canada (Froese and Moreno 2006) and at the Åknes rock slope site in western Norway (Blikra et al. 2005).

The lessons learned from the Randa installation demonstrate that in many cases, the geological, geotechnical, and hydrogeological field and instrumentation data often cited as being necessary to constrain complex numerical analyses are similarly affected by the same issues of rock mass complexity and variability as the methods they are meant to constrain. Field mapping and instrumentation data provided important input and constraints for the numerical models used to investigate the instability mechanism at Randa, but numerical modelling also provided a means to constrain the interpretation of deformation measurements with respect to identifying potential instability scenarios in relation to different sliding surface configurations.

Finally, it must be emphasized that numerical modelling is only a tool and not a substitute for critical thinking and engineering (or geological) judgement. Still, the potential exists to use numerical modelling to build upon empirical methodologies to improve the visualization and comprehension of the coupled processes and complex mechanisms driving rock slope failures. By better integrating the different data sets collected, geological uncertainty can be minimized and controlled with respect to the comprehension of complex rock slope failure mechanisms. In doing so, it is hoped that meaningful and much needed advances in rockslide hazard assessment and forecasting will be made thereby increasing our ability to effectively assess, monitor, mitigate, and predict the potential for catastrophic failure.

Acknowledgments

The author wishes to acknowledge and thank his many colleagues who have been involved with various aspects of the work presented in this Colloquium paper, especially the graduate students who helped contribute to the material presented: Dr. Heike Willenberg, Alex Strouth, and Dr. Tom Spillmann. The Randa study and In situ Rockslide Laboratory involved a large multidisciplinary effort with key contributions from Dr. Heike Willenberg, Prof. Simon Loew, Prof. Doug Stead, Dr. Keith Evans, Dr. Hansruedi Mauer, Dr. Tom Spillmann, Prof. Alan Green, Dr. Björn Heincke, Dr. John Coggan, Prof. Peter Kaiser, Stump Messtechnik, Injectoboh/SIF, Beat Rinderknecht, Christoph Bärlocher, and Franz Gönner. Further acknowledgement is extended to Prof. Oldrich Hungr for his contributions to the written manuscript. This work was made possible through funding provided in part by the Swiss National Science Foundation and the Natural Sciences and Engineering Research Council of Canada.

References

Bhasin, R., and Kaynia, A.M. 2004. Static and dynamic simulation of a 700-m high rock slope in western Norway. Engineering Geology, **71**(3–4): 213–226. doi:10.1016/S0013-7952(03)00135-2.

Blikra, L.H., Longva, O., Harbitz, C., and Løvholt, F. 2005. Quantification of rock-avalanche and tsunami hazard in Storfjorden, western Norway. *In* Landslides and Avalanches, Proceedings of the 11th International Conference and Field Trip on Landslides (ICFL), Norway, 1–10 September 2005. *Edited by* K. Senneset, K. Flaate, and J.O. Larsen. Taylor & Francis Group, London. pp. 57–64.

Board, M., Chacon, E., Varona, P., and Lorig, L. 1996. Comparative analysis of toppling behaviour at Chuquicamata open-pit mine, Chile. Transactions of the Institution of Mining and Metallurgy Section A-Mining Industry, **105**: A11–A21.

Bonzanigo, L., Eberhardt, E., and Loew, S. 2007. Long-term investigation of a deep-seated creeping landslide in crystalline rock. Part 1. Geological and hydromechanical factors controlling the Campo Vallemaggia landslide. Canadian Geotechnical Journal, **44**(10): 1157–1180. doi:10.1139/T07-043.

Brunsden, D. 1979. Mass movements. *In* Process in geomorphology. Edward Arnold, London. pp. 130–186.

Chryssanthakis, P., and Grimstad, E. 1996. Landslide simulation by using the distinct element method. *In* Rock Mechanics: Tools and Techniques, Proceedings of the 2nd North American Rock Mechanics Symposium (NARMS '96), Montréal, 19–21 June 1996. *Edited by* M. Aubertin, F. Hassani, and H. Mitri. A.A. Balkema, Rotterdam. Vol. 2. pp. 1921–1928.

Collins, B.D., and Znidarcic, D. 2004. Stability analyses of rainfall induced landslides. Journal of Geotechnical and Geoenvironmental Engineering, **130**: 362–372. doi:10.1061/(ASCE)1090-0241(2004)130:4(362).

Costa, M., Coggan, J.S., and Eyre, J.M. 1999. Numerical modelling of slope behaviour of Delabole slate quarry (Cornwall, UK). International Journal of Surface Mining, Reclamation and Environment, **13**(1): 11–18. doi:10.1080/09208119908944196.

Crosta, G.B., and Agliardi, F. 2003. Failure forecast for large rock slides by surface displacement measurements. Canadian Geotechnical Journal, **40**(1): 176–191. doi:10.1139/t02-085.

Dawson, E.M., Roth, W.H., and Drescher, A. 1999. Slope stability analysis by strength reduction. Géotechnique, **49**: 835–840.

Duncan, J.M. 2000. Factors of safety and reliability in geotechnical engineering. Journal of Geotechnical and Geoenvironmental Engineering, **126**: 307–316. doi:10.1061/(ASCE)1090-0241(2000)126:4(307).

Eberhardt, E., and Willenberg, H. 2005. Using rock slope deformation measurements to constrain numerical analyses, and numerical analyses to constrain rock slope deformation measurements. *In* Proceedings of the 11th International Conference on Computer Methods and Advances in Geomechanics, Torino. *Edited by* G. Barla and M. Barla. Pàtron Editore, Bologna, Vol. 4, pp. 683–692.

Eberhardt, E., Stead, D., and Stimpson, B. 1999. Quantifying progressive pre-peak brittle fracture damage in rock during uniaxial compression. International Journal of Rock Mechanics and Mining Sciences, **36**(3): 361–380. doi:10.1016/S0148-9062(99)00019-4.

Eberhardt, E., Willenberg, H., Loew, S., and Maurer, H. 2001. Active rockslides in Switzerland - Understanding mechanisms and processes. *In* International Conference on Landslides - Causes, Impacts and Countermeasures, Davos, 17–21 June 2001. *Edited by* H.H. Einstein, E. Krauter, H. Klapperich, and R. Pöttler. Verlag Glückauf Essen, Essen. pp. 25–34.

Eberhardt, E., Stead, D., and Coggan, J.S. 2004*a*. Numerical analysis of initiation and progressive failure in natural rock slopes – the 1991 Randa rockslide. International Journal of Rock Mechanics and Mining Sciences, **41**(1): 69–87. doi:10.1016/S1365-1609(03)00076-5.

Eberhardt, E., Spillmann, T., Maurer, H., Willenberg, H., Loew, S., and Stead, D. 2004*b*. The Randa Rockslide Laboratory: Establishing brittle and ductile instability mechanisms using numerical modelling and microseismicity. *In* Landslides: Evaluation and Stabilization, Proceedings of the 9th International Symposium on Landslides, Rio de Janeiro, 28 June – 2 July 2004. *Edited by* W.A. Lacerda, M. Ehrlich, S.A.B. Fontoura, and A.S.F. Sayão. A.A. Balkema, Leiden, Vol.1, pp. 481–487.

Eberhardt, E., Thuro, K., and Luginbuehl, M. 2005. Slope instability mechanisms in dipping interbedded conglomerates and weathered marls - the 1999 Rufi landslide, Switzerland. Engineering Geology, **77**(1–2): 35–56. doi:10.1016/j.enggeo.2004.08.004.

Evans, S.G. 2006. Single-event landslides resulting from massive rock slope failure: characterizing their frequency and impact on society. *In* Landslides from massive rock slope failure. *Edited by* S.G. Evans, G. Scarascia Mugnozza, A. Strom, and R.L. Hermanns. Springer, Dordrecht. pp. 53–73.

Feng, J., Chuhan, Z., Gang, W., and Guanglun, W. 2003. Creep modeling in excavation analysis of a high rock slope. Journal of Geotechnical and Geoenvironmental Engineering, **129**(9): 849–857. doi:10.1061/(ASCE)1090-0241(2003)129:9(849).

Fredlund, D.G., and Krahn, J. 1977. Comparison of slope stability methods of analysis. Canadian Geotechnical Journal, **14**(3): 429–439.

Froese, C., and Moreno, F. 2006. Turtle Mountain Field Laboratory (TMFL): Part 1 - Concept and Research Activities. *In* Geo2006: Proceedings of the 59th Canadian Geotechnical Conference and 7th Joint CGS/IAH-CNC Groundwater Specialty Conference, Vancouver, 1–4 October 2006. BiTech Publishers, Richmond, B.C. pp. 544–551.

Fukuzono, T. 1985. A new method for predicting the failure time of a slope. *In* Proceedings of the 4th International Conference and Field Workshop on Landslides, Tokyo. National Research Center for Disaster Prevention, Tokyo. pp. 145–150.

Griffiths, D.V., and Lane, P.A. 1999. Slope stability analysis by finite elements. Géotechnique, **49**(3): 387–403.

Hajiabdolmajid, V., and Kaiser, P.K. 2002. Slope stability assessment in strain-sensitive rocks. *In* EUROCK 2002, Proceedings of the ISRM International Symposium on Rock Engineering for Mountainous Regions, Funchal, Madeira, 25–28 November 2002. *Edited by* C. Dinis da Gama and L. Ribeiro e Sousa. Sociedade Portuguesa de Geotecnia, Lisboa, pp. 237–244.

Hart, R.D. 1993. An introduction to distinct element modeling for rock engineering. *In* Comprehensive rock engineering: Principles, practice & projects. Pergamon Press, Oxford. pp. 245–261.

Heim, A. 1932. Bergsturz und Menschenleben. Fretz and Wasmuth Verlag, Zurich. pp. 218. [In German.]

Heincke, B. 2005. Determination of 3-D fracture distribution on an unstable mountain slope using georadar and tomographic seismic refraction techniques. D.Sc. thesis, Applied and Environmental Geophysics, Swiss Federal Institute of Technology, ETH Zurich.

Hungr, O. 1995. A model for the runout analysis of rapid flow slides, debris flows, and avalanches. Canadian Geotechnical Journal, **32**(4): 610–623. doi:10.1139/t95-063.

Hungr, O., and Evans, S.G. 2004. The occurrence and classification of massive rock slope failures. Felsbau, **22**(2): 16–23.

Hungr, O., Corominas, J., and Eberhardt, E. 2005. Estimating landslide motion mechanism, travel distance and velocity. *In* Landslide risk management. *Edited by* O. Hungr, R. Fell, R. Couture and E. Eberhardt. A.A. Balkema, Leiden. pp. 99–128.

Ischi, H., Keusen, H.R., and Scheller, E. 1991. Randa, Kt. Wallis: Bergsturz Grossgufer vom April/Mai 1991 - Zusammenfassender Bericht über die Aktivitäten der Geotest AG. Report #91126, Geotest AG, Martigny. [In German.]

Itasca. 2005. FLAC/Slope - Advanced factor-of-safety determination for rock and soil slopes in two dimensions (Ver. 5.0). Itasca Consulting Group, Minneapolis, Minn.

Jaboyedoff, M., Baillifard, F., Couture, R., Derron, M.H., Locat, J., and Locat, P. 2005. Coupling kinematic analysis and sloping local base level criterion for large slope instabilities hazard assessment - a GIS approach. *In* Landslide risk management. *Edited by* O. Hungr, R. Fell, R. Couture, and E. Eberhardt. A.A. Balkema, Leiden. pp. 615–622.

Kemeny, J. 2003. The time-dependent reduction of sliding cohesion due to rock bridges along discontinuities: A fracture mechanics approach. Rock Mechanics and Rock Engineering, **36**(1): 27–38. doi:10.1007/s00603-002-0032-2.

Kennedy, B.A., and Niermeyer, K.E. 1970. Slope monitoring systems used in the prediction of a major slope failure at the Chuquicamata Mine, Chile. *In* Planning Open Pit Mines, Proceedings, Johannesburg, 29 August – 4 September 1970. *Edited by* P.W.J. Van Rensburg. A.A. Balkema, Cape Town. pp. 215–225.

Lee, E.M., and Jones, D.K.C. 2004. Landslide risk assessment. Thomas Telford, London. 454 pp.

Lo, K.Y., and Lee, C.F. 1973. Stress analysis and slope stability in strain-softening materials. Géotechnique, **23**(1): 1–11.

Löw, S. 1997. Wie sicher sind geologische Prognosen? Bulletin für Angewandte Geologie, **2**: 83–97. [In German.]

Martin, C.D. 1997. Seventeenth Canadian Geotechnical Colloquium: The effect of cohesion loss and stress path on brittle rock strength. Canadian Geotechnical Journal, **34**(5): 698–725. doi:10.1139/cgj-34-5-698.

McDougall, S., and Hungr, O. 2004. A model for the analysis of rapid landslide motion across three-dimensional terrain. Canadian Geotechnical Journal, **41**(6): 1084–1097. doi:10.1139/t04-052.

Muller, J.A., and Martel, S.J. 2000. Numerical models of translational landslide rupture surface growth. Pure and Applied Geophysics, **157**(6–8): 1009–1038. doi:10.1007/s000240050015.

Munjiza, A., Owen, D.R.J., and Bicanic, N. 1995. A combined finite-discrete element method in transient dynamics of fracturing solids. Engineering Computations, **12**: 145–174. doi:10.1108/02644409510799532.

Nichol, S.L., Hungr, O., and Evans, S.G. 2002. Large-scale brittle and ductile toppling of rock slopes. Canadian Geotechnical Journal, **39**(4): 773–788. doi:10.1139/t02-027.

O'Connor, K.M., and Dowding, C.H. 1999. GeoMeasurements by pulsing TDR cables and probes. CRC Press, Boca Raton, Fla. 424 pp.

Peck, R.B. 1969. Advantages and limitations of the observational method in applied soil mechanics. Géotechnique, **19**(2): 171–187.

Rocscience. 2006. Phase 2 - finite element analysis for excavations and slopes (Ver. 6.0). Rocscience Inc., Toronto, Ont.

Rose, N.D., and Hungr, O. 2007. Forecasting potential rock slope failure in open pit mines using the inverse-velocity method. International Journal of Rock Mechanics and Mining Sciences, **44**(2):308–320. doi:10.1016/ijmms.2006.07.014.

Saito, M. 1965. Forecasting the time of occurrence of a slope failure. *In* Proceedings of the 6th International Conference on Soil Mechanics and Foundation Engineering, Montréal. University of Toronto Press, Toronto. Vol. 2, pp. 537–541.

Salt, G. 1988. Landslide mobility and remedial measures. *In* Proceedings of the 5th International Symposium on Landslides, Lausanne. *Edited by* C. Bonnard. A.A. Balkema, Rotterdam. Vol.1, pp. 757–762.

Sartori, M., Baillifard, F., Jaboyedoff, M., and Rouiller, J.-D. 2003. Kinematics of the 1991 Randa rockslides (Valais, Switzerland). Natural Hazards and Earth System Sciences, **3**: 423–433.

Scavia, C. 1995. A method for the study of crack propagation in rock structures. Géotechnique, **45**(3): 447–463.

Scheidegger, A.E. 1973. On the prediction of the reach and velocity of catastrophic landslides. Rock Mechanics, **5**: 231–236. doi:10.1007/BF01301796.

Schindler, C., Cuénod, Y., Eisenlohr, T., and Joris, C.-L. 1993. Die Ereignisse vom 18. April und 9. Mai 1991 bei Randa (VS) - ein atypischer Bergsturz in Raten. Eclogae Geologicae Helvetiae, **86**: 643–665.

Shou, K.-J., and Wang, C.-F. 2003. Analysis of the Chiufengershan landslide triggered by the 1999 Chi-Chi earthquake in Taiwan. Engineering Geology, **68**: 237–250. doi:10.1016/S0013-7952(02)00230-2.

Spillmann, T. 2007. Borehole radar experiments and microseismic monitoring on the unstable Randa rockslide (Switzerland). D.Sc. thesis, Applied and Environmental Geophysics, Swiss Federal Institute of Technology (ETH Zurich).

Stacey, T.R. 1981. A simple extension strain criterion for fracture of brittle rock. International Journal of Rock Mechanics and Mining Sciences and Geomechanics Abstracts, **18**(6): 469–474. doi:10.1016/0148-9062(81)90511-8.

Stacey, T.R., Xianbin, Y., Armstrong, R., and Keyter, G.J. 2003. New slope stability considerations for deep open pit mines. Journal of the South African Institute of Mining and Metallurgy, **103**(6): 373–389.

Stead, D., and Eberhardt, E. 1997. Developments in the analysis of footwall slopes in surface coal mining. Engineering Geology, **46**(1): 41–61. doi:10.1016/S0013-7952(96)00084-1.

Stead, D., Eberhardt, E., and Coggan, J.S. 2006. Developments in the characterization of complex rock slope deformation and failure using numerical modelling techniques. Engineering Geology, **83**: 217–235. doi:10.1016/j.enggeo.2005.06.033.

Stroth, A.B. 2006. Integrated use of terrestrial laser scanning and advanced numerical methods for a "Total Slope Analysis" of Afternoon Creek, Washington. M.A.Sc. thesis, Geological Engineering/EOS, The University of British Columbia, Vancouver, B.C.

Stroth, A., and Eberhardt, E. 2006. The use of LiDAR to overcome rock slope hazard data collection challenges at Afternoon Creek, Washington. *In* Proceedings of the 41st U.S. Symposium on Rock Mechanics, Golden. American Rock Mechanics Association, [CD-ROM], CD: 06–993.

Stroth, A., Burk, R.L., and Eberhardt, E. 2006. The Afternoon Creek Rockslide near Newhalem, Washington. Landslides, **3**(3): 175–179. doi:10.1007/s10346-005-0030-z.

Terzaghi, K. 1950. Mechanism of landslides. *In* Application of geology to engineering practice (Berkey volume). Geological Society of America, New York. pp. 83–123.

Wagner, A. 1991. Bergsturz Grossgufer Randa: Etude structurale et géomécanique. CRSFA/91.35, Centre de Recherches Scientifiques Fondamentales et Appliquées de Sion, Sion.

Willenberg, H. 2004. Geologic and kinematic model of a complex landslide in crystalline rock (Randa, Switzerland). D.Sc. thesis, Engineering Geology, Swiss Federal Institute of Technology (ETH Zurich).

Willenberg, H., Evans, K.F., Eberhardt, E., and Loew, S. 2003. Monitoring of complex rock slope instabilities – correction and analysis of inclinometer/extensometer surveys and integration with surface displacement data. *In* Proceedings of the 6th International Symposium on Field Measurements in Geomechanics, Oslo. *Edited by* F. Myrvoll. A.A. Balkema, Lisse. pp. 393–400.

Willenberg, H., Loew, S., and Eberhardt, E. 2004*a*. Hangstabilität und Gefahrenanalyse der Alpe di Roscioro (Preonzo, TI). Expert Report/Geologischer Bericht: No. ETH 3465/45, ETH Zurich, Zurich.

Willenberg, H., Loew, S., Eberhardt, E., Evans, K.F., Spillmann, T., Heincke, B., Maurer, H., and Green, A. 2008*a*. Internal structure and deformation of an active slope instability in crystalline rock above Randa (Switzerland): Part I - Internal structure from integrated geological and geophysical investigations. Engineering Geology. In Press. doi:10.1016/j.enggeo.2008.01.015.

Willenberg, H., Evans, K.F., Eberhardt, E., Spillmann, T., and Loew, S. (2008*b*). Internal structure and deformation of an active slope instability in crystalline rock above Randa (Switzerland): Part II ? Three-dimensional deformation pattern. Engineering Geology: In Press. doi: doi:10.1016/j.enggeo.2008.01.016..

Wong, F.S. 1984. Uncertainties in FE modeling of slope stability. Computers & Structures, **19**(5/6): 777–791. doi:10.1016/0045-7949(84)90177-9.

Wyllie, D.C., and Mah, C.W. 2004. Rock slope engineering. 4th ed. Spon Press, London. 431 pp.

Zienkiewicz, O.C. 1971. The finite element method in engineering science. McGraw-Hill, London. 521 pp.

Zienkiewicz, O.C., Humpheson, C., and Lewis, R.W. 1975. Associated and non-associated visco-plasticity and plasticity in soil mechanics. Géotechnique, **25**(4): 671–689.

Zvelebil, J. 1984. Time prediction of a rockfall from a sandstone rock slope. *In* Proceedings of the 4th International Symposium on Landslides, Toronto. University of Toronto Press, Toronto, Ont., 16–21 September 1984. Vol. 3, pp. 93–95.